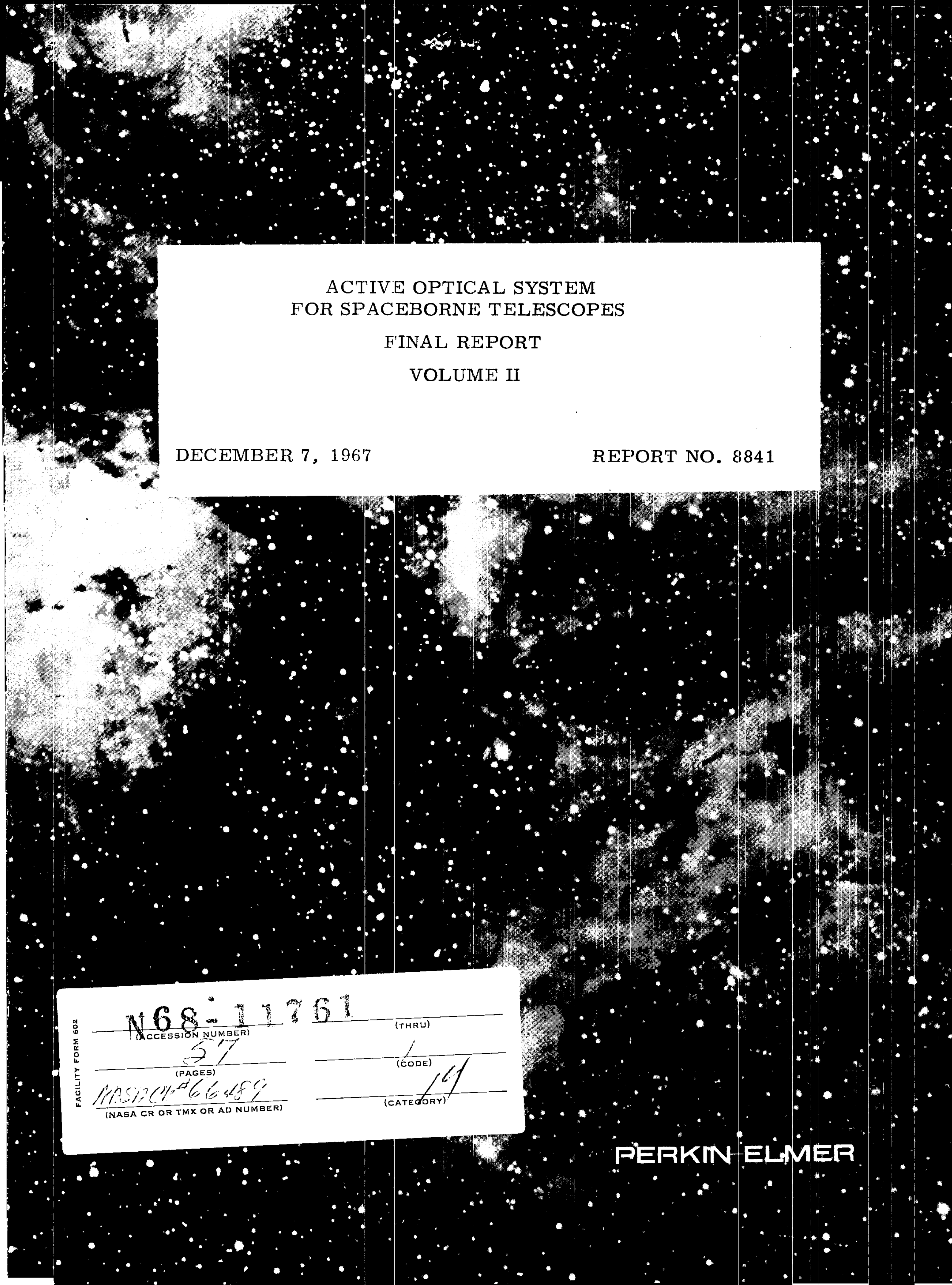

ACTIVE OPTICAL SYSTEM FOR SPACEBORNE TELESCOPES

FINAL REPORT

VOLUME II

DECEMBER 7, 1967

REPORT NO. 8841

PERKIN-ELMER

NASA CR-66489

PERKIN-ELMER

OPTICAL GROUP NORWALK, CONNECTICUT

ENGINEERING REPORT NO. 8841

ACTIVE OPTICAL SYSTEM FOR SPACEBORNE TELESCOPES
FINAL REPORT

VOLUME II

DATE: December 7, 1967

Distribution of this report is provided in the interest of information exchange. Responsibility for the contents resides in the authors or organization that prepared it.

PREPARED FOR: NATIONAL AERONAUTICS AND SPACE ADMINISTRATION
LANGLEY RESEARCH CENTER
LANGLEY STATION
HAMPTON, VIRGINIA 23365

CONTRACT NUMBER: NAS1-5198 CCN 1 PROJECT NUMBER: SPO 27563

H. J. Robertson, Project Manager

H. S. Hemstreet, Director, Advanced Systems

Contributors:

R.A. Arnold
R. Crane, Jr.
R.C. Liu
H.J. Robertson

ACTIVE OPTICAL SYSTEM FOR SPACEBORNE TELESCOPES

FINAL REPORT

VOLUME II

By H.J. Robertson, R. Crane, Jr.
R.C. Liu, and R.A. Arnold

ABSTRACT

A refinement of the control technique, described in Volume I (NASA CR-66297) for actively controlling rigid segments of a telescope primary mirror, is given. The refined concept allows the figure error sensor to integrate over a large portion of each segment to average out small surface irregularities and provides a degree of immunity to mechanical transients. Using this technique, the figure error of the composite 20-inch mirror was significantly reduced.

PRECEDING PAGE BLANK NOT FILMED.

TABLE OF CONTENTS

LIST OF ILLUSTRATIONS

LIST OF ILLUSTRATIONS (Con't)

LIST OF TABLES

1. SUMMARY

The segmented Active Optics system has been modified to provide automatic tilt alignment, to provide a degree of immunity to mechanical transients, and to allow more accurate alignment of the composite mirror. The control system has been optimized and further data has been obtained to determine the system performance and its limits of accuracy.

Automatic control of the segment alignment has again produced near diffraction limited performance as demonstrated by independent pinhole imaging. Alignment accuracy is estimated to be better than 1/50 wavelength rms. Dynamic stability has been measured to be better than 1/100 wavelength rms. The control system will now accommodate an external transient, such as that introduced by a person leaning on the vacuum tank assembly, with only a mild reaction and no loss of control.

2. OBJECTIVES

The Active Optics program has shown that modern optical technology can be combined with closed-loop servo-control techniques to provide and maintain a large diffraction-limited mirror surface for use in an orbiting astronomical telescope. The concept of continuous active control was first demonstrated with a composite mirror made up of mirror segments which were oriented and maintained in alignment to diffraction-limited tolerances. The results of the experiment to demonstrate the feasibility of this system were reported in Perkin-Elmer Report No. 8525 "Active Optical System for Spaceborne Telescopes - Final Report".

In order to make an accurate comparison between the segmented system, the active deformable thin mirror system now under investigation (NASA Contract No. NAS 1-7104), and the traditional thick monolithic mirror, as candidates for a large spaceborne orbiting astronomical telescope, it was necessary to obtain additional data to further our understanding of the experimental capability of the segmented system. In particular, it was desirable to determine the performance parameters of the system operation, including alignment accuracy, stability, and dynamic rates. Of interest also was the further automation of the system to provide a degree of immunity to mechanical transients and to provide an automatic alignment ability which would allow the system to recover from the effects of severe mechanical shocks.

The initial Active Optics control system did not have the ability to automatically sense and remove alignment errors of magnitude greater than one half wavelength introduced by mechanical transients. It is necessary to have a self-correcting system that can live within its environment, including any transient effects. For this reason, a revised control logic system has been developed.

Initial misalignment errors are apt to be quite large compared to the final accuracy required. It is therefore desirable to have a system in which response rates are fast in the presence of large errors, and slow and stiff when alignment is close to being correct. These new requirements may be summarized as a need for an automatic adaptive control system, that is, one which can automatically adapt its error sensing and control rate to the size of the alignment errors.

Test data on the overall figure error of the composite Active Optics mirror assembly showed that the original system was vulnerable to localized figure errors of relatively large peak value which happen to occur at the exact spot in front of the actuators. This was because actuation control signals were generated by looking at this spot only, relative to a reference spot. For example, Figure 42 in the Final Report No. 8525 shows that spot No. 6 falls near a turned up edge, with the result that segment II was not aligned optimumly in tilt about the 4-5 axis. Peak errors occurring in the figure sensor can be equally disturbing. To obtain a closer fit of the mirror segments with the ideal sphere, it is desirable to sense the average figure error over an area of the mirror rather than at one spot.

This report describes the changes made in the original segmented Active Optics system to improve its performance and it discusses the results of the measurements made on the final system to determine its accuracy.

The results show that the limit of accuracy of the control system is better than that required to maintain the $\lambda/50$ rms alignment needed for diffraction limited performance in the visible spectrum. The alignment accuracy and limiting factors are discussed in detail in Section 5.3.

The overall objective of the additional studies performed under this Contract Change Notice as set forth in the contract Statement of Work was to "Evaluate the segmented optical system by measuring and isolating the factors which determine the system accuracy and dynamic rate, making those modifications necessary to determine the fundamental limits".

The specific objectives spelled out in the contract and the sections of this report which contain the corresponding results of the investigation are as follows:

	Statement of Work	Report Section
A.	Automate certain portions of the tilt alignment sequencing to demonstrate the feasibility of operating the control system under moderate transient inputs such as might be experienced in manned orbiting telescopes.	Section 4
B.	Obtain improved quality knife-edge photographs after eliminating present spurious reflections from the system.	Section 5.2
C.	Improve system performance by eliminating anomalies due to the measuring system such as beamsplitter distortions and scanning spot locations.	Sections 3 & 4
D.	Repeat raster scan mapping of the mirror surface after making above improvements.	Section 5.2

The development and operation of the figure sensor, the actuators, the mirror and its support system, and the original electronic control system are described in Perkin-Elmer Reports 8255 and 8525, the Phase I and Final Reports on "Active Optical System for Spaceborne Telescopes". Most of this information has been omitted from the present report in the interest of brevity. It may be necessary, therefore, to refer to the previous reports to more fully understand some of the details of this report.

3. INTERFEROMETER MODIFICATIONS

In the process of optimizing the overall system, a number of modifications were made in the interferometer (Figure 1). There were four types of modifications performed: (1) replacement of those optical components generating measurable figure error; (2) stabilization of those component mounts observed to be unstable; (3) cleaning of the optical elements; and (4) modification, where possible, of component mounts in order to accomplish proper alignment more conveniently and accurately.

3.1 REDUCTION OF FIGURE ERROR

In the first class of modification, two elements within the interferometer were replaced. It was observed that the beamsplitter was astigmatic to the extent of a $\lambda/40$ variation at the perimeter of the aperture. A replacement beamsplitter was selected which removed this aberration.

The second element replaced was the pinhole located in the beam-expanding telescope. This pinhole is used as a spatial filter to remove diffraction structure in the laser output and allow the use of an inexpensive microscope objective for the short focal length lens in the telescope. In the operation of a Twyman Greene interferometer, half the illuminating energy returns to the source as distinguished from going to the output image. This energy is focused by the long focal length lens in the beam-expanding telescope to a small image on the pinhole material, which then acts as a weak second source. This could not be attenuated in the present application by the usual method utilizing a quarter-wave plate and a polarizer, because this would upset the operation of the phase measurement interferometer. It was possible however, to reduce this effect significantly by selecting a pinhole material with a minimum reflectivity from the side toward the interferometer. The modification did not remove the secondary source, but did reduce its intensity to a level which causes little observable effect.

A third optical element, external to the interferometer, was also replaced. This was the small flat mirror used to direct (upward to the microscope) the illumination which forms the image of the test pinhole. The replacement mirror obtained was figured to $\lambda/50$ over an area much larger than the required aperture. With this mirror, freedom to vary the location of the mirror relative to the pinhole image has been increased without degrading the image. This has been of great advantage in the knife-edge test where the knife edge must be in the image plane and the mirror a substantial distance from the image.

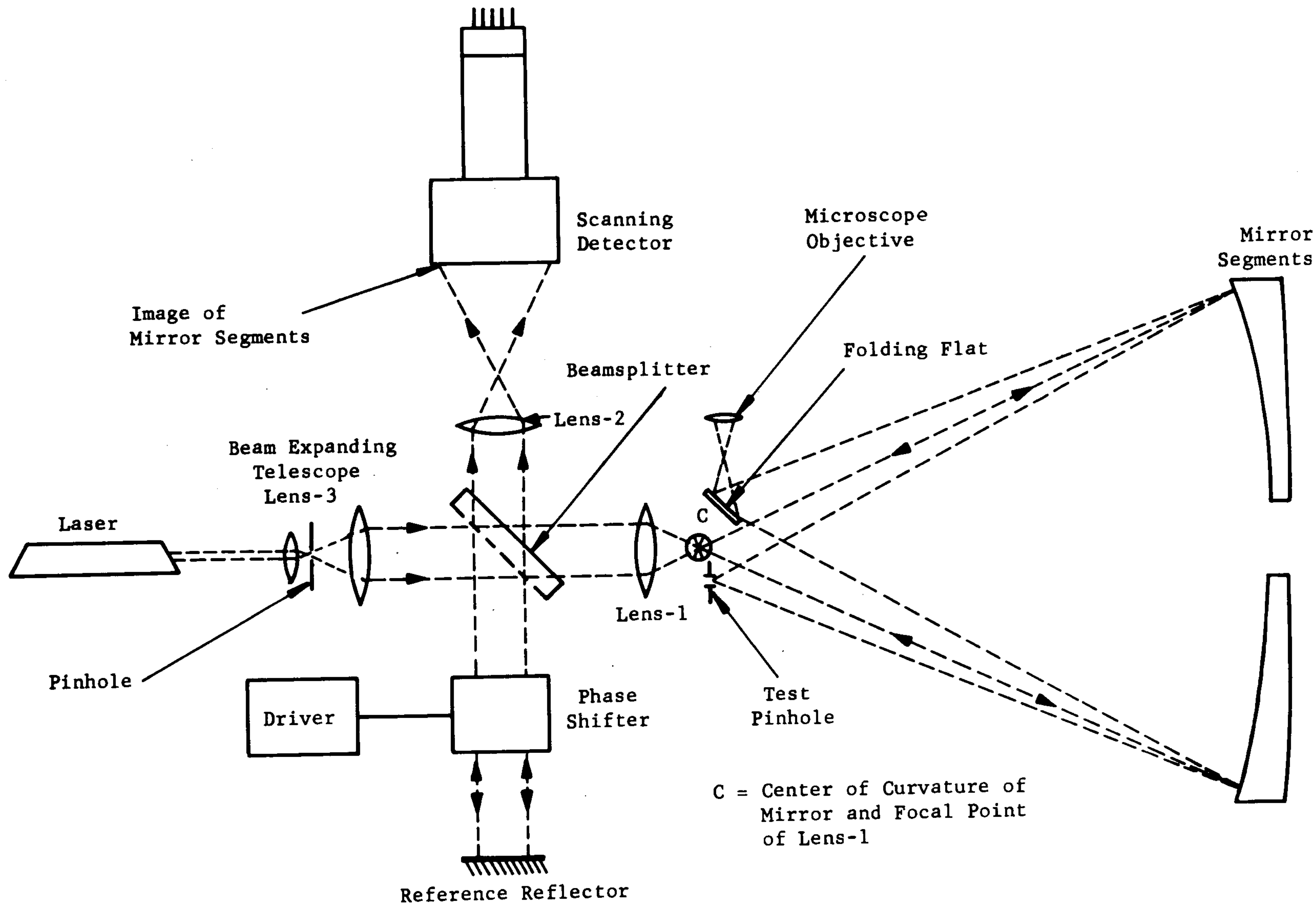

Figure 1. Phase-Measuring Interferometer Arrangement

3.2 COMPONENT STABILIZATION

During the normal operation of the system, only one component mount was observed to be of inadequate stability. This was the assembly consisting of the pinhole mount and illuminating system. In operation, the illuminating lamp would raise the temperature of the housing considerably. As the pinhole and mounting points were at opposite ends of the assembly, the thermal expansion would translate the pinhole sideways several thousandths of an inch. The effect of this was that, until thermal equilibrium had been reached, which required considerable time, the image of the pinhole would be slowly moving and would appear distorted when photographed with long exposure. Additionally, this effect severely hampered obtaining good knife-edge test photographs. Very long exposure times are required due to the large image of the mirror formed in this test. During these exposures, the image of the pinhole would move either completely off the knife edge or become completely obstructed by it and the proper adjustment would be lost. By redesigning the mount, the pinhole source could be supported quite near the pinhole itself. In this configuration, no motion of the pinhole has been detected.

3.3 ELEMENT CLEANING

An additional area in which work was done was in respect to cleaning. A dust particle within the optical path in the interferometer scatters the illumination and acts as a weak coherent source. This scattered light interferes with the unscattered light and creates a weak, but observable, phase and intensity variation pattern in the final interference image. This phase variation then appears in the output data as attributed to test mirror figure error. To reduce this source of error, all optical elements within the interferometer were cleaned in accordance with directed procedures for the various surface coatings. This was done at the same time that the pinhole was replaced and, because of the small magnitude of the original effects, no quantitative data was taken to evaluate the improvements. Visual observations of the image pattern indicated that the undesired effects were reduced, and no evidence of them is now seen in the raster scans.

3.4 MODIFICATIONS FOR ALIGNMENT

Several component mounts were modified to facilitate optimum alignment of the interferometer. The housing containing the beam expander, short focal length lens and the spatial filter pinhole was modified to allow better control over the position of the pinhole relative to the lens. This allows adjustment for maximum illumination. The mounting of the long focal length lens was also modified to allow it to be independently adjusted to give a good plane wavefront from the beam expander. When the pinhole image folding mirror was replaced, a new mount was provided for it and for the knife edges used in the Foucault test. This mount allows the associated elements to be more conveniently manipulated into the desired positions for various observations.

3.5 MEASURED PERFORMANCE

Figure 2 is a copy of a set of data taken to evaluate the performance of the interferometer. This data is a set of raster scan measurements of the image formed at the scanning detector taken with a precision flat mirror mounted in place of the decollimating lens and segmented mirror shown in figure 1. When these measurements were taken, there was no active control keeping the mirror aligned. It is observed that the second measurement, marked "Finish", at the bottom of the page has changed the equivalent of $\lambda/50$ in the lower region of the aperture relative to the center of the aperture during the ten minutes required to complete the measurements. This is caused by thermal drift of the interferometer. The small ripple of the trace of about $\lambda/100$ peak-to-peak is near the resolution limit for this system, based on the illumination level utilized, the detector quantum efficiency, the number of multiplexed information channels, and the recorder response time constant.

The curvature of the profiles, indicated by the solid lines drawn through the raster scans in figure 2, is caused by a slight curvature of the wavefront as it leaves the beam expanding telescope (lens 3 in figure 1). The curvature observed represents a mispositioning of approximately 0.0005 inches in the spacing of the two elements of lens 3. It could be removed entirely by adjusting the element spacing exactly; however, the system can accommodate small amplitudes of spherical curvature of the wavefront by adjusting the spacing of the decollimating lens (Lens 1 in Fig. 1) and the segmented mirror, without introducing an error in the positioning of the mirror segments.

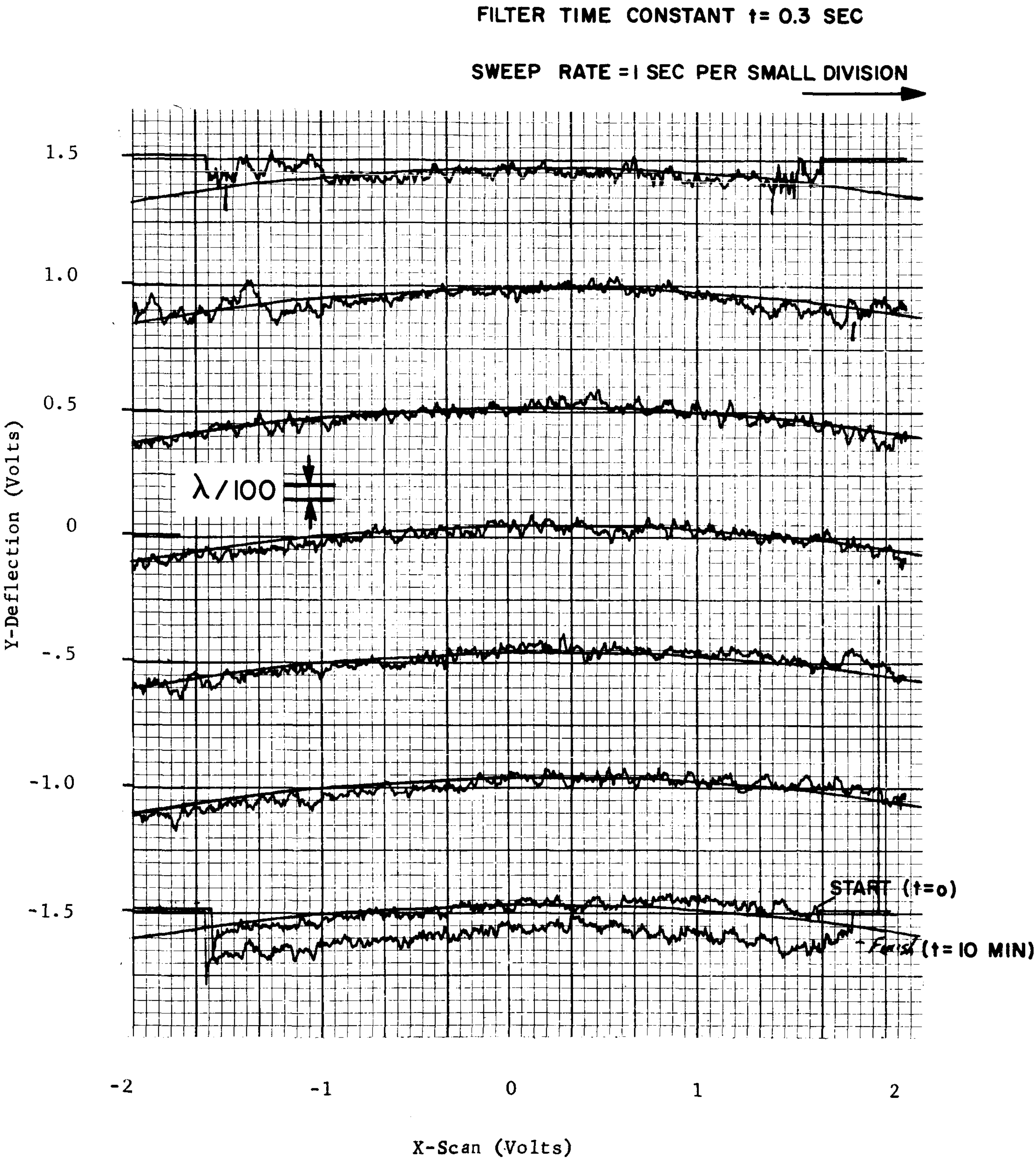

Figure 2. Raster Scan of Phase Measuring Interferometer, Using Reference Flat in Measuring Arm (Smooth Curve = Zero Wavefront Deformation)

4. CONTROL SYSTEM MODIFICATION

4.1 APPROACH

The objectives of the work on the control system were to provide a system which would accomodate moderate transient inputs and make it possible to determine the fundamental limits of performance. The selected approach consists of:

a. Automation of portions of the alignment sequence.

b. Averaging of alignment errors in both time and space.

c. Introduction of a degree of adaptive control.

The control system may be divided into ten modules: Control Logic, Scan Generator, Electro-Optical Scanner, Interferometer, Ambiguity Sensor, Electronic Amplifiers and Phase Detectors, Switching Networks, Stabilization Networks, Servo Amplifiers, and Actuators. Figure 3 shows the interrelationship between these modules. The scanner, ambiguity sensor, servo amplifiers, and actuators were used from the original experiment. A small modification was made on the actuators. This is described in paragraph 4.2.5. The amplifier and phase detector principles of operation were not changed; however new circuitry was constructed. The phase dectector circuit is described in Section 4.2.3 as an example of the circuitry used. New control logic, scan generator, switching networks, and stabilization networks were devised. These are described in Sections 4.2.1, 4.2.2, 4.2.4, and 4.3. The reader is referred to PE Report 8255 for descriptions of the unmodified modules used from the original experiment.

The approach to the modified control system is best described in terms of the new scan pattern for the interferometer fringe pattern scanner. In the modified experiment a circular scan covers one segment at a time. The circle diameter is controlled by an AGC so that in the presence of a large alignment error, the circle is small; and conversely, when alignment is correct, the circle size is large. The scanner is also electronically commutated at a very high rate back and forth between the circumference and the center of the circle. The circle center is used as a reference spot for the phase detectors which are used in sensing alignment errors. Alignment errors are measured by comparing the fringe pattern phase at the circle circumference with the phase at the center. This gives a large amount of space-averaging compared to the

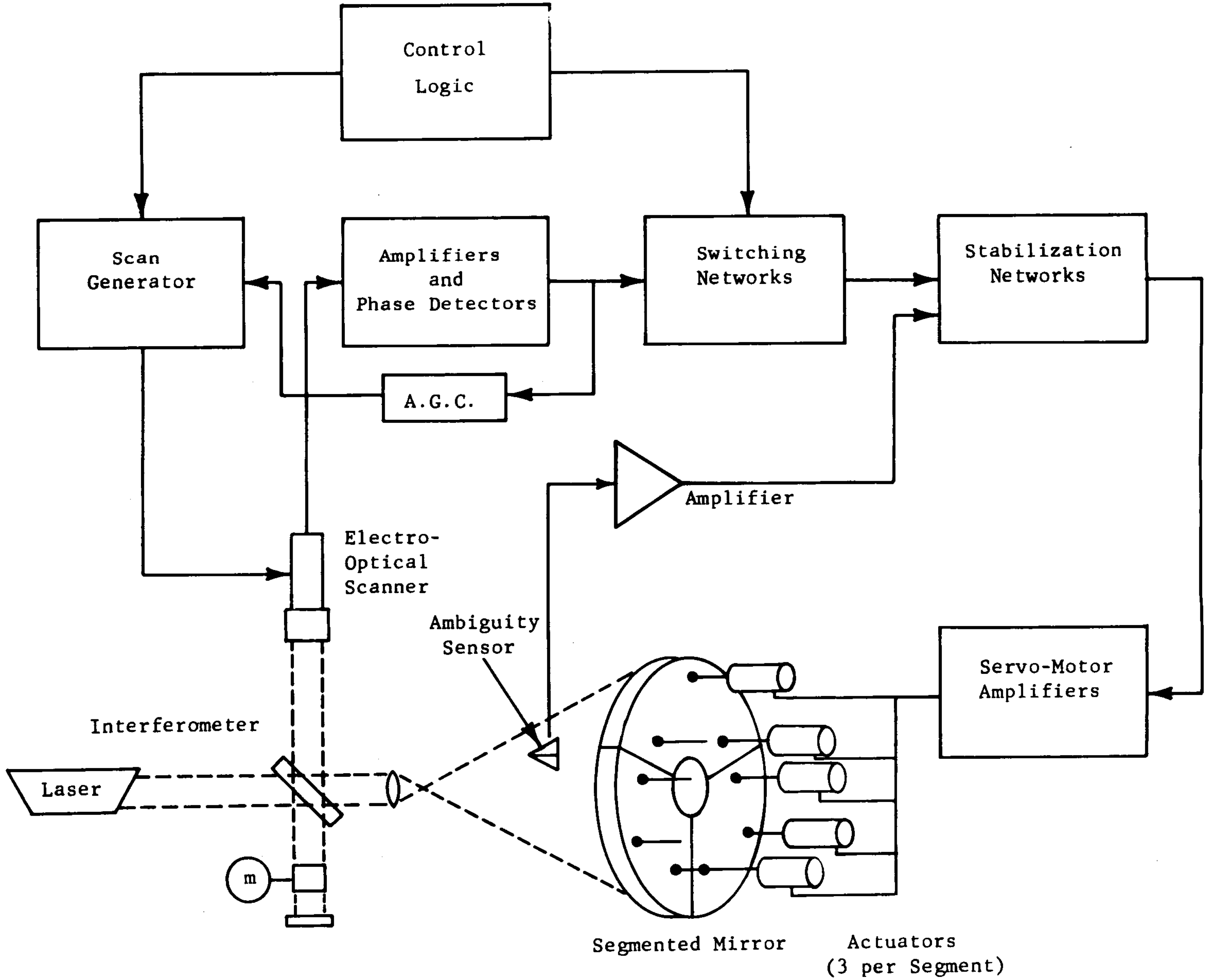

Figure 3. Experimental Arrangement Block Diagram

single spot measurements used originally. Each circular scan simultaneously generates alignment error data for three control channels: two tilt axes and one axial or focus channel.

The circular scan and its center spot are stepped from one segment to the next at a three step-per-second rate. Thus control signals are generated for all nine actuator channels each second. These alignment error voltages are routed to the appropriate control channel by switching networks in which the switching is synchronized with the circular scan by a control logic module.

The modified approach corrects for tilt by push-pull action, with the axis of mirror rotation passing through a spot corresponding to the center of the scan circle. Axial control for a particular segment is obtained by simultaneously driving all three actuators in the same direction. Thus, there is no crosstalk between channels.

The stabilization networks consist of long time-constant, low-pass filters to provide time averaging of the figure errors. Time constants on the order of ten seconds are used. This, in combination with the automatic scan size control, gives a high degree of immunity to transients. It was also necessary to include compensation networks in all channels to provide adequate phase margin for closed-loop control. A discussion of the control loop as a servo system is given in Section 4.3.

Because tilt, focus, and axial alignment errors are generated simultaneously, and because there is minimum crosstalk between control channels, it is now possible in principle to perform alignment in only two steps. The first step brings all segments into tilt alignment and segment I into focus alignment. The second step brings segments II and III onto a common reference sphere concentric with segment I. Furthermore, time and spatial averaging have improved the accuracy of the alignment and considerably reduced the effects of external transients.

4.2 DESCRIPTION

Figure 4 is a functional diagram of the electronic portions of the modified Active Optics experiment. The major elements in Figure 4, corresponding to the modules of Figure 2, are identified by boxed titles and are enclosed in dotted lines. The flow of error data and control signals is indicated by heavy arrows. A number of electronic switches are indicated by the symbol shown at the right, where a = input, c = output, and b = control lead.

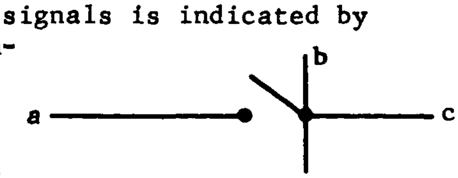

The electronic functions performed by the modules in Figure 4 will now be discussed, and examples of the circuitry used will be given.

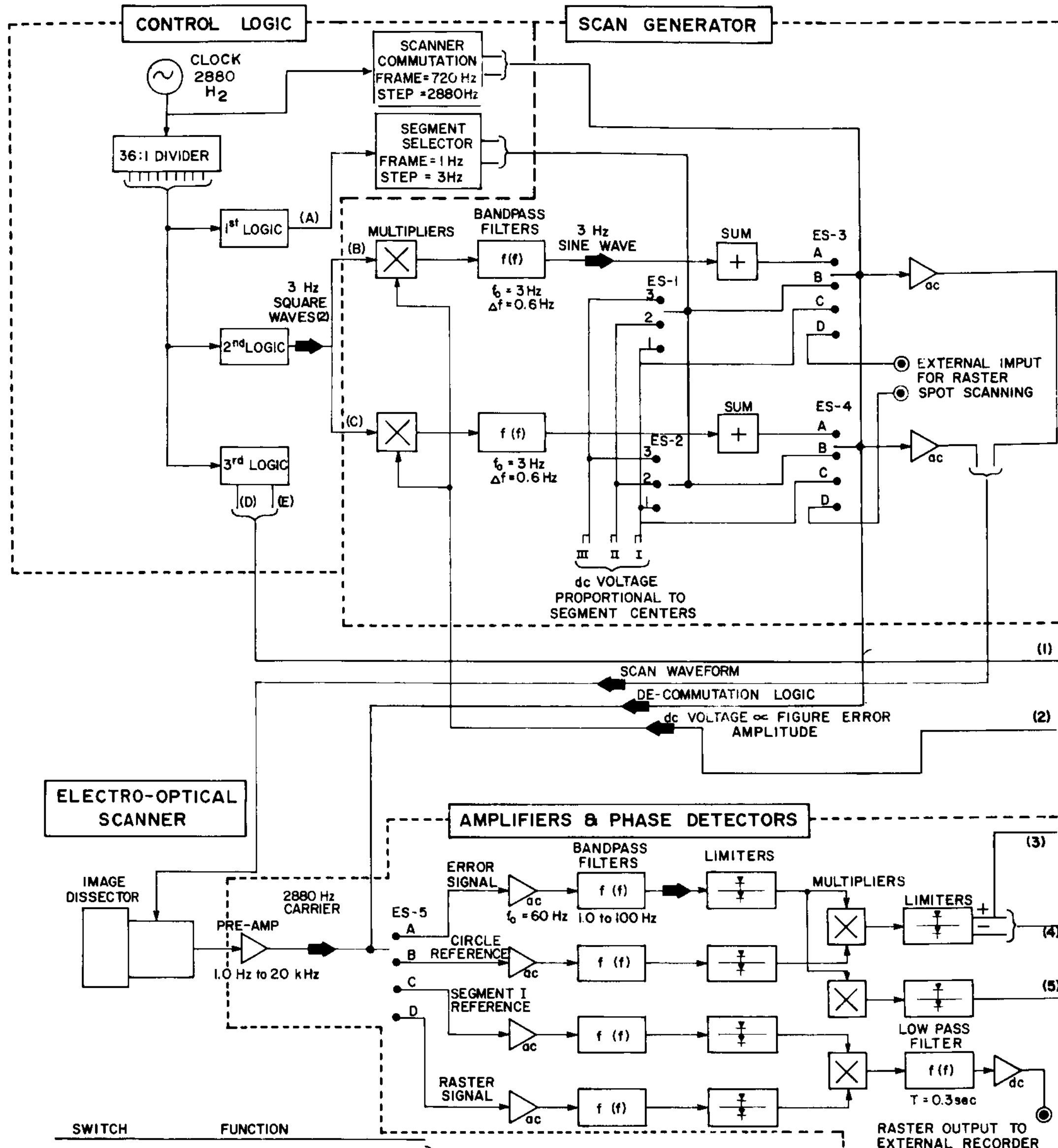

SWITCH	FUNCTION	
MS-1	POWER ON—OFF	NOT SHOWN
MS-2	400 Hz POWER ON—OFF	NOT SHOWN
MS-3	WHITE LIGHT INTERFEROMETER DC POWER ON—OFF	NOT SHOWN
MS-4	FOCUS CHANNEL ON—OFF	
MS-5	SEGMENT II AXIAL CONTROL ON-OFF	
MS-6	SEGMENT III AXIAL CONTROL ON-OFF	
MS-7	AXIAL SLEW 1 - OFF 2 - SEG. II 3 - SEG. III	
MS-8	AXIAL SLEW DIRECTION	

MS = MANUAL SWITCH
ES = ELECTRONIC SWITCH
RS = RELAY

ELECTRONIC SWITCH LOGIC

SWITCH	FUNCTION	STEP	POSITION
ES-1,2	SWEEP POSITIONING	1 2 3	SEGMENT I SEGMENT II SEGMENT III
ES-3,4	SCANNER COMMUTATION	A B C D	CIRCULAR SWEEP CIRCLE CENTER SEGMENT I CENTER EXTERNAL RASTER SCAN
ES-5	SCANNER DE-COMMUTATION	A B C D	FIGURE ERROR SIGNAL CIRCLE CENTER REFERENCE SEGMENT I REFERENCE RASTER SIGNAL

ES-6 thru 14 (see table I)

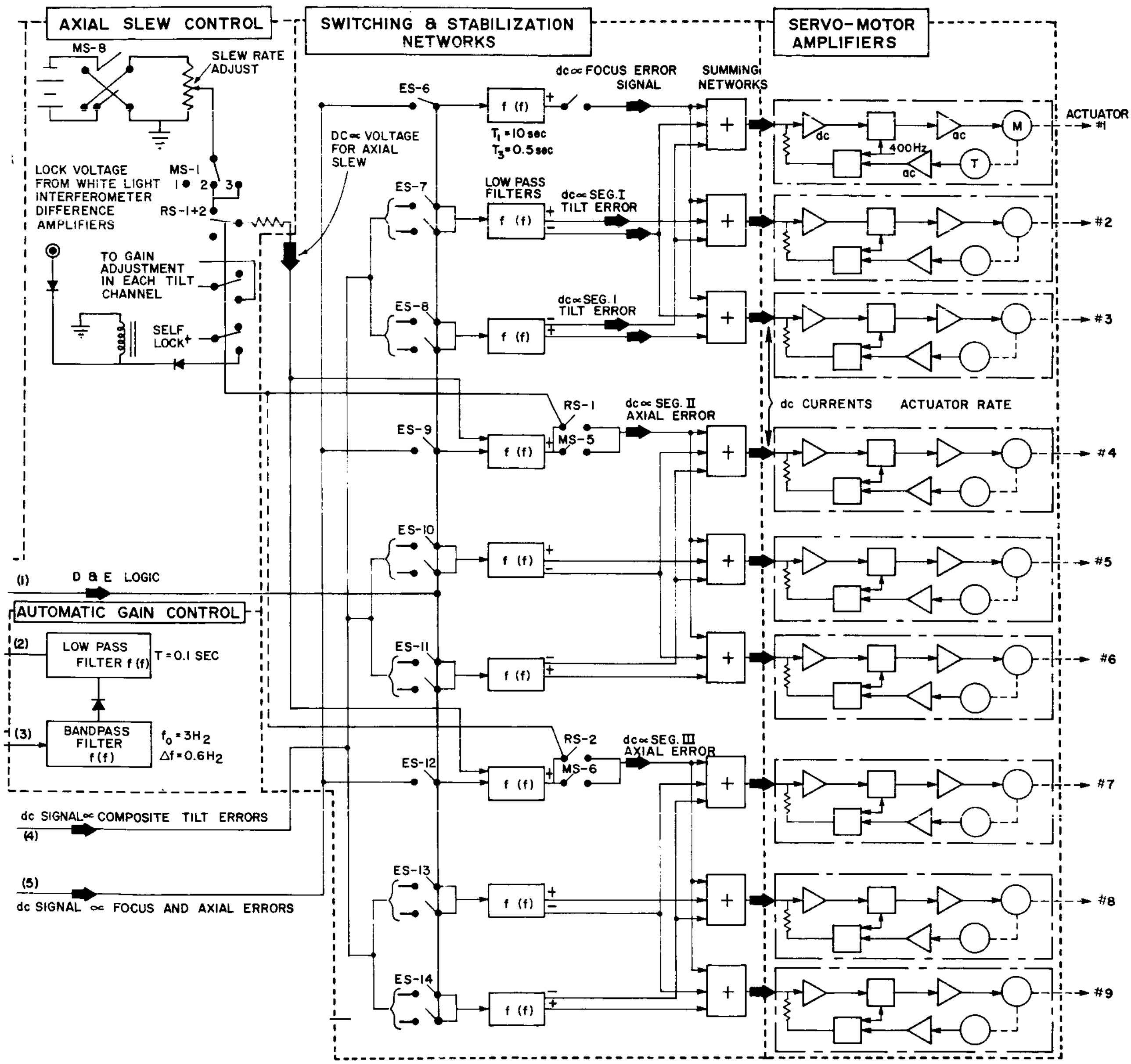

Figure 4. Function Diagram, Modified Active Optics Experiment

4.2.1 Control Logic Module

This module creates timing waveforms for the scan generator and synchronized gates that control the switching networks.

The control logic module is keyed to a 2880 Hz clock shown in the upper left-hand corner of figure 4 (sheet 1 of 2). This frequency is fed directly to the scanner to control its rapid commutation between circles and center spots. The same waveforms control the decommutation of the scanner output signal via switch ES-5. The 2880 Hz is also fed to a series of dividers which count down to one Hz. Several waveforms are extracted from the dividers and fed to three logic networks.

The first logic network performs segment selection for the scanner sweep. Three segments are sampled sequentially in a 1-second frame period at a three step-per-second rate. The second logic network generates two 3 Hz square waves separated in phase by 90°, from which a circular scan is generated. The third logic network generates control gates for the error switching networks. These gates are referred to as "D and E logic" in figure 4. The switches operate in synchronism with the fringe pattern scan so that tilt, axial, and focus alignment errors are routed to the correct control channel.

An understanding of the synchronism between the scan waveform and error signal switching can best be obtained by referring to figure 5. This shows the scan pattern, with maximum circle diameter, superimposed upon an outline of the segmented mirror. Also shown are the positions of the actuators behind the mirror. The dot-dash lines are the axes of rotation for the tilt motions. For example, channel 2 tilt alignment rotates segment I about a line parallel to a line between actuators 1 and 3 and passing through the center of the scan circle. The numerals about the periphery of the circles represent 36 time bins per scan frame period of one second. During the first 12 time bins, alignment errors are measured for segment I: bins 1 to 12 generate focus data, bins 1, 12, 11, 10 and 9 generate tilt errors for channel 2, bins 3, 4, 5, 6 and 7 generate tilt errors for the same channel, which are inverted and added to the tilt errors from bins 1, 12, 11, 10 and 9. Similarly, error signals are generated for the other tilt axis. Thus, one circular scan generates alignment error data for three control channels for a single segment.

The circular scan steps sequentially from one segment to the next. It is therefore necessary to switch a sample of the measured alignment error data to the proper control channel in accordance with the time bin relationship implied by figure 5. The exact switching logic is listed in table I. The numbers in table I correspond to the 36 time bins shown in figure 5. The "positive" and "negative" categories in table I indicate time bins during which the measured alignment error sense will be positive or negative. Time gates corresponding to the time bin logic of table I are referred to as "D & E Logic" and are used to control the switching network module.

Examples of the circuitry used to generate the D and E logic are given in figures 6 and 7. The waveforms of figure 6 (a) are extracted from

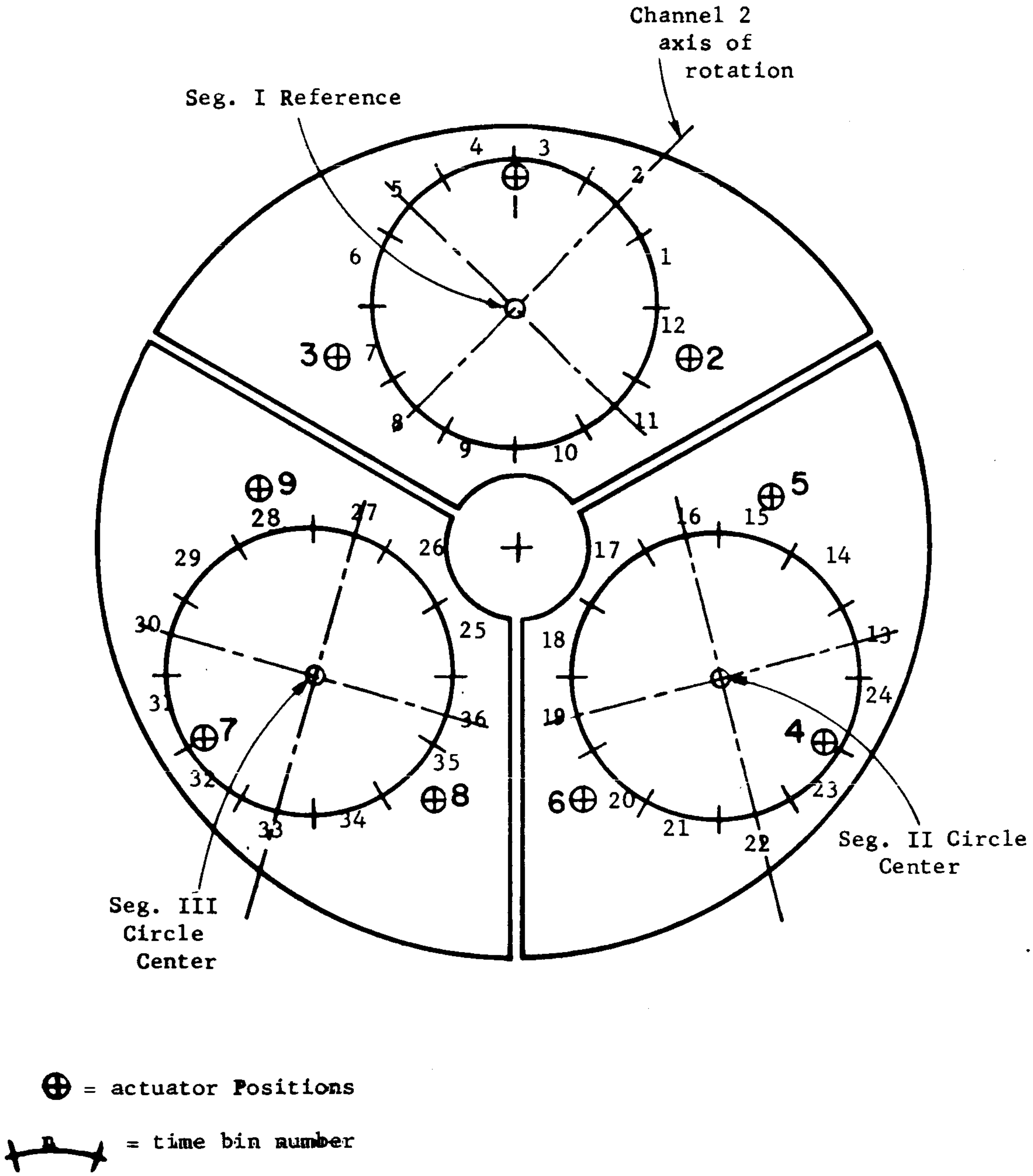

Figure 5. Image Dissector Scan Pattern

TABLE I. D AND E LOGIC

Segment	Focus	Axial Alignment	Actuator 2, 5, or 8 Tilt	Actuator 3, 6 or 9 Tilt
I	1-12	-	Positive: 1, 9-12 Negative: 3-7	Positive: 6-10 Negative: 1-4, 12
II	-	13-24	Positive: 14-18 Negative: 20-24	Positive: 17-21 Negative: 13-15, 23, 24
III	-	25-36	Positive: 25, 26, 34-36 Negative: 28-32	Positive: 25-29 Negative: 31-35

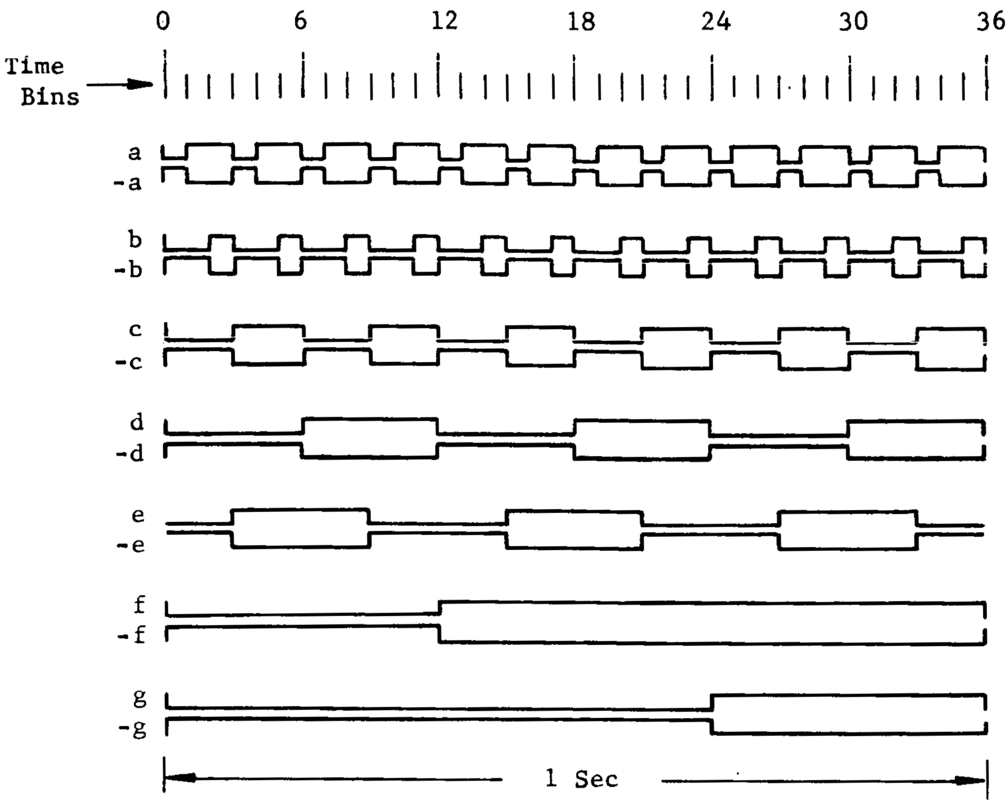

(a) 36:1 Divider Output Waveforms

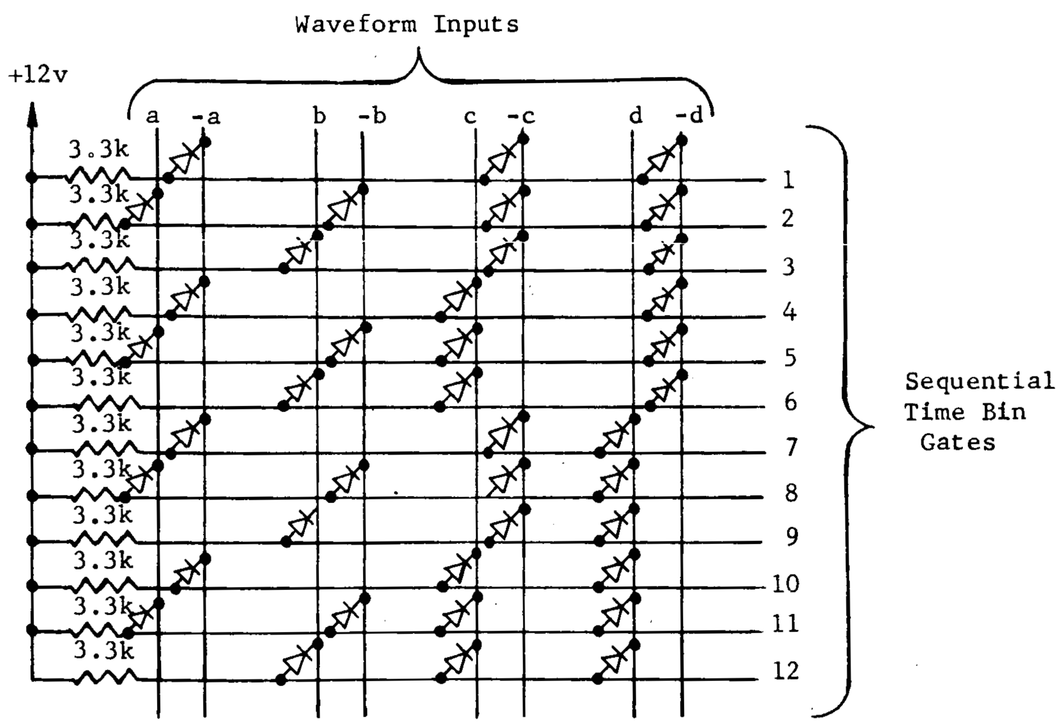

(b) Diode Logic for Generating Sequential Time Bin Gates

Figure 6. Diode Logic Matrix

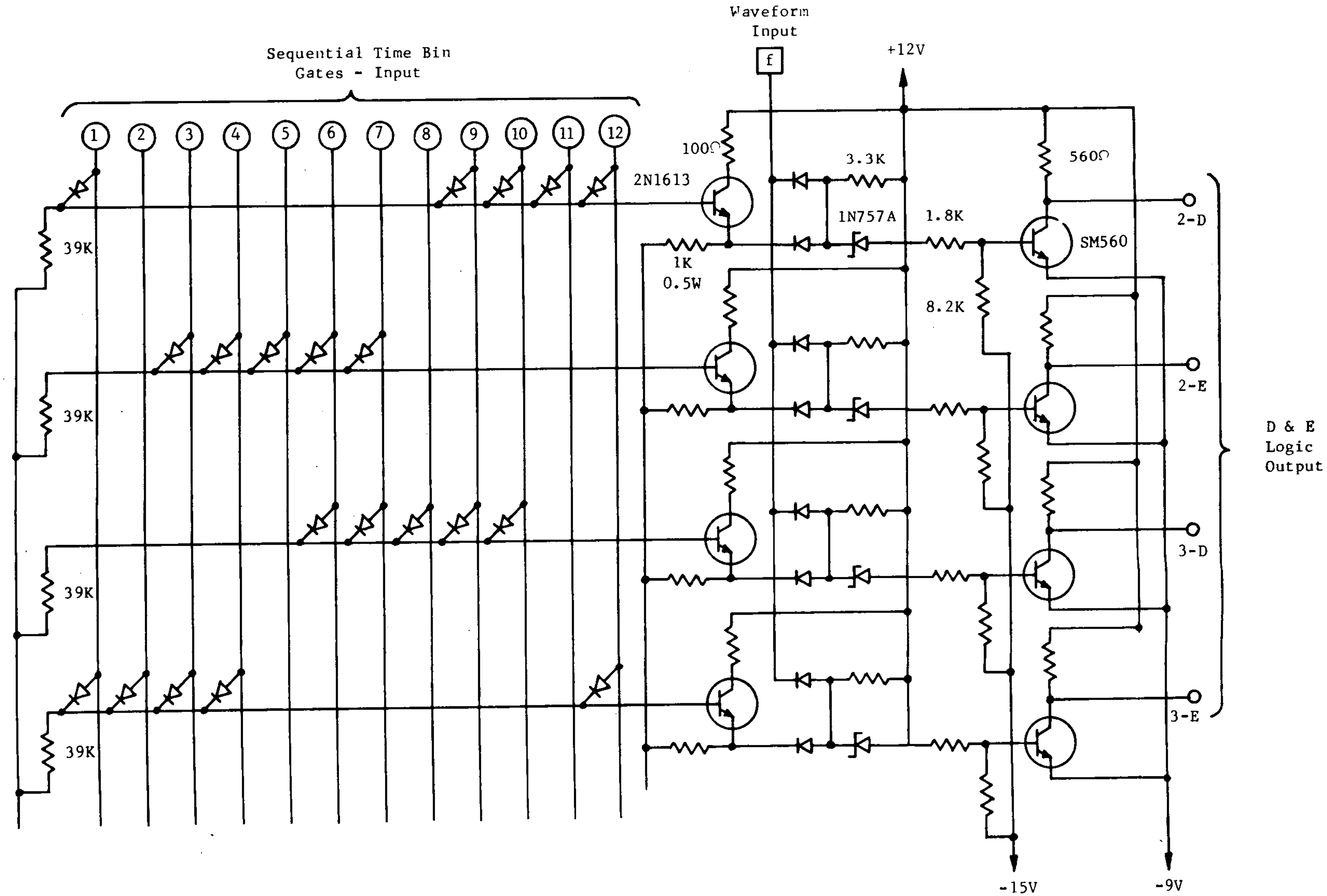

Figure 7. D and E Logic Generator

the dividers. These are combined by the diode logic of 6 (b) to produce sequential time bin gates ; one gate for each of the first 12 bins is produced by the circuitry shown. These are then combined as shown in figure 7 to produce D and E logic waveforms. Control waveforms for channels 2 and 3 only are produced by the circuitry shown. Altogether 15 waveforms make up the D and E logic, and these control the 15 electronic switches in the switching network module (figure 4, sheet 2) which are labeled "ES-6 thru ES-14". The actual waveform of the D & E logic is shown in figure 8.

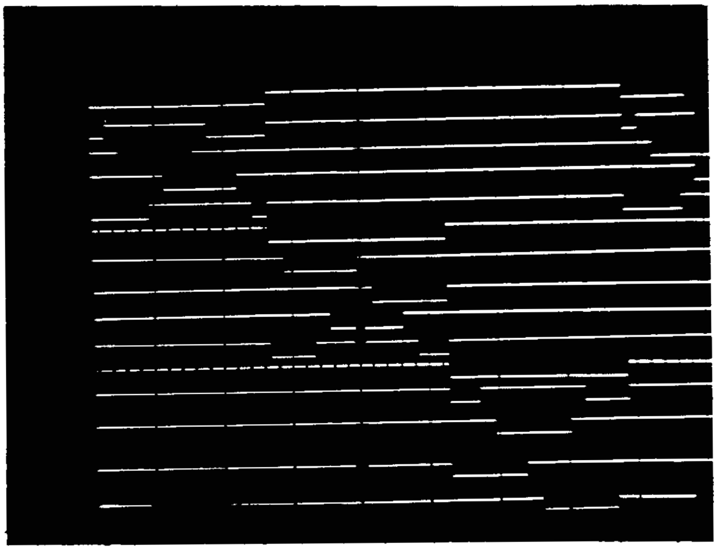

Figure 8. D and E Logic Waveforms

4.2.2 Scan Generator Module

The scan generator module generates deflection waveforms for the control of the electro-optical scanner. The waveforms must cause the scanner to sample the interferometer fringe pattern so that nine alignment error signals can be extracted. This is done by a combination of circular scans of each segment with phase reference spots at the center of each circle.

The control logic module feeds two square waves, separated in phase by 90°, to the scan generator. These are fed to two multipliers, at which point the amplitude is adjusted by an AGC voltage between the values of 15 percent and 100 percent. The two extremes of scan amplitude correspond to dimensions on the mirror of 1 and 7 inch diameter. This adjustment of the scan diameter is necessary because the figure sensor error voltage becomes ambiguous in the presence of large alignment errors. To accomodate this factor, the scan is controlled by the AGC circuit to restrict the scan size to cover less than one fringe in the interferometer pattern. The AGC voltage is derived by a detector at the phase detector output which responds to any 3 Hz component in the measured alignment error voltage.

The 3 Hz square wave sweep voltages are passed through bandpass filters which pass only the fundamental frequency. Two sinewaves are produced, with a relative phase of 90°, which generate a circular scan when fed to the X and Y deflection channels. The sinewaves are then summed with a d-c voltage corresponding to the center of each segment. This d-c voltage is automatically cycled by the segment selector switches ES-1 and 2. Figure 9 shows the scan deflection waveforms at this point.

It is necessary to commutate the scan voltage with three other voltages before sending it to the scanner deflection circuitry. The scanner commutator, ES-3 and 4, operates at a step rate of 2880 steps per second and a frame rate of 720 Hz. There are four scan channels provided in the system. Channel A is for the circular scan, channel B samples three center spots (one for each segment), channel C samples a spot at the center of segment I, which is used as the fundamental reference point, and channel D is controlled by an external voltage. Figure 10 shows the scan pattern including the three circles and three center spots. Also visible in the figure is the effect of the 2880 Hz commutation of the scanner.

4.2.3 Phase Detectors

Alignment errors appear as variations of relative phase in the interferometer fringe pattern. The phase shifter in the interferometer converts the fringe pattern to a sinusoidally fluctuating pattern, at a 60 Hz rate. This is converted to a 60 Hz electronic signal by the electro-optical scanner. Therefore, alignment errors become variations in phase of a 60 Hz carrier as the scanner looks at various positions in the fringe pattern corresponding to various points on the mirror surface.

Since the scanner is commutated between four types of scan, the electronic signal is a composite of four data samples. The electronic signal is, therefore, divided into four separate channels by the decommutation switch ES-5. These four channels are identified in figure 4 as: A = error signal, B = circle reference, C = segment I reference, D = raster signal.

Alignment error signals for tilt control are obtained by detecting phase differences between channels A and B. Axial and focus error signals are obtained from channels A and C. Channel D contains a signal corresponding to an externally controlled spot which may be located anywhere on the mirror for checking alignment of the segments, with channel C as the reference.

The output of each phase detector is directly proportional to the cosine of the phase angle between the reference and signals under investigation. It is therefore necessary to introduce a 90° phase shift between signal and reference channels so that the phase detector output will have both sign and amplitude directly related to phase difference. This is provided by shifting the error signal and reference signal by plus and minus 45° respectively with simple RC networks.

In order to reject incidental amplitude modulation which might exist in the signal and also to obtain a linear function of the phase difference,

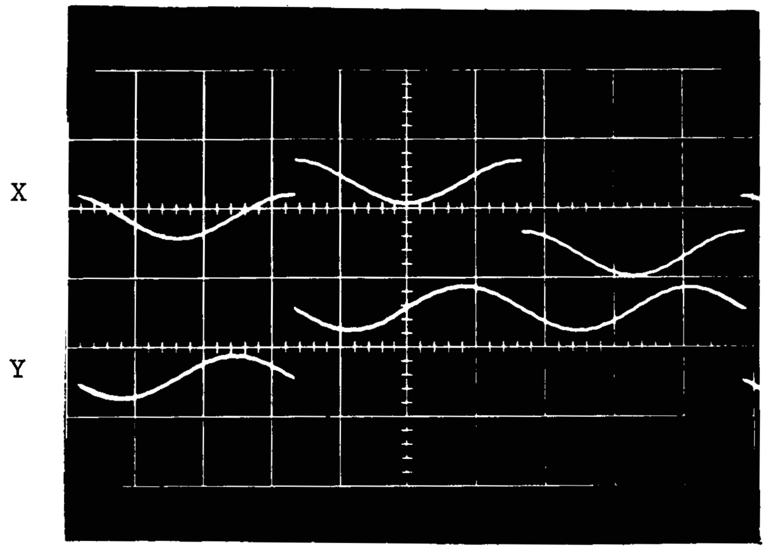

Figure 9. Circular Scan Deflection Waveforms

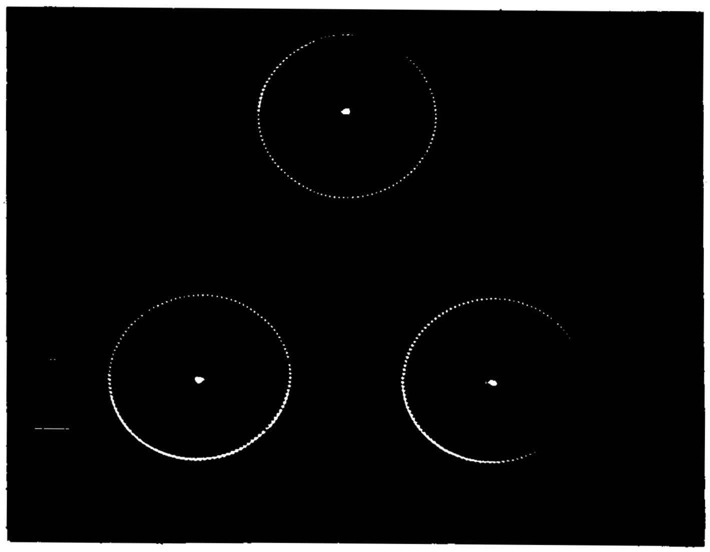

Figure 10. Monitored Circular Scan

the input signal to the phase detector is hard limited. In the circuit of figure 11, the large voltage gain and wide dynamic range of the operational amplifier allow a sharp transition at zero crossing with a symmetrical, clean, and flat-topped output waveform. Note that a zener diode is used for bridging. Input signals of ±25 mv drive the output to limiting voltage as determined by the zener voltage.

Square wave signals from the limiters are applied to the phase detectors. These produce rectangular wave outputs in which the positive (or negative) duty cycle is directly proportional to the phase difference between the two input signals.

An example of the phase detector circuit is shown in figure 12. A pair of complementary transistors is used in conjunction with an operational amplifier. The switching transistors are operated in an inverted mode to minimize offset. When a positive reference voltage is applied, the NPN transistor is ON and the PNP transistor is OFF. Thus, the operational amplifier inverts the signal to

$$e_o = -e_i \frac{R_2}{R_1}$$

With a negative reference voltage, the situation will be reversed and the amplifier output becomes

$$e_o = e_i \frac{R_2}{R_1 + R_2} \times \frac{R_1 + R_2}{R_1} = e_i \frac{R_2}{R_1}$$

Thus, full-wave demodulation is achieved by switching the amplifier back and forth from negative to positive amplification.

4.2.4 Switching Networks

The switching networks, shown in figure 4, accept alignment error signals from the phase detectors, D & E switching signals from the control logic, and slew voltages from the axial slew control. From these, via appropriate combinations of switching and summations, control signals are generated for each actuator.

Focus error signals control all three actuators in segment I. Tilt error signals cause push-pull operation of all three actuators controlling the segment concerned. Axial control of segments II and III is derived initially from a manually adjusted slew control. When the white light interferometers indicate that segment II is cospherical with segment I, relay RS-1 is activated. This causes axial alignment to be maintained via error voltages from the phase detectors described in Section 4.2.3. The same sequence, employing RS-2, is used for segment III.

The filter and stabilization networks are described in the servo system discussion of Section 4.3.

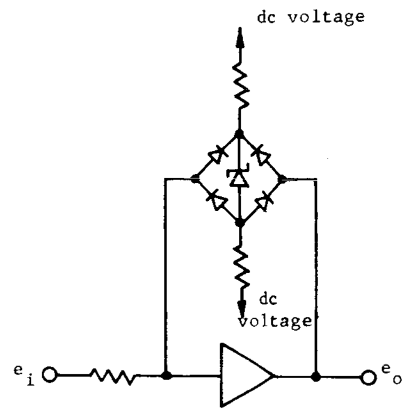

Figure 11. Hard Limiter Circuit

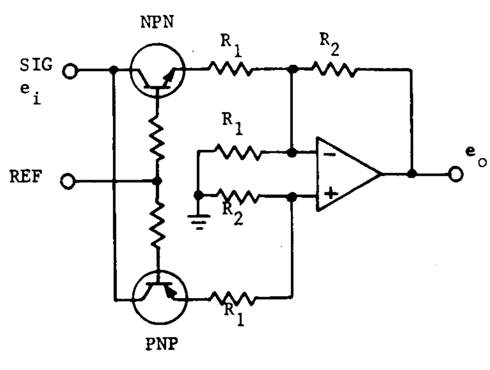

Figure 12. Phase Detector Circuit

4.2.5 Actuators

During the troubleshooting phase of the work, unstable control loop operation was encountered. This was found to be caused by geartrain spring windup and unsymmetrical damping in the actuators. In some cases, 35° to 50° of unanticipated phase lag was found. Modification of the soft spring in the actuators was required to obtain adequate performance. Figure 13 shows typical actuator responses for poor and good operation.

4.3 SERVO SYSTEM

The objectives of the modified servo design were to provide: 1) adequate gain for acceptable overall accuracy, 2) sufficient integration to nullify the effects of external transients, and 3) adequate phase margin to give an overdamped time response. The servo design will be described in terms of one tilt control loop. The same considerations, with different numerical values, apply for the focus and axial control.

A servo diagram for one tilt control loop (see figure 14) shows the important elements considered. These will now be discussed briefly. The sensor transfer function is such that the phase ϕ_e or ϕ_r of the 60 Hz carrier is related to the mirror surface position in the Z axis by

$$\phi = 1.2\pi \frac{Z_d - Z_o}{\lambda}$$

which has a numerical value of

$$\phi = 5.4 \times 10^4 \ Z_e$$

As stated earlier, the sensor is commutated between the mirror area of interest and a reference spot in the center of each segment, thus both ϕ_e and ϕ_r are generated. The sensor also has a multiplicative noise source caused by photon noise in the laser illumination.

The error and reference channels have matching filters. These eliminate the scan commutation frequency and also provide initial photon-noise filtering. This is necessary to prevent signal-times-noise cross products in the phase detector which might otherwise cause serious suppression of the signal.

The phase detector generates a d-c voltage (e_e) proportional to the phase difference between the signal and reference carrier:

$$e_e = K_d \left(\phi_r - \phi_e\right)$$

$$= \pm 5.7 \left(\phi_r - \phi_e\right) \frac{\text{Vdc}}{\pi \text{rad}}$$

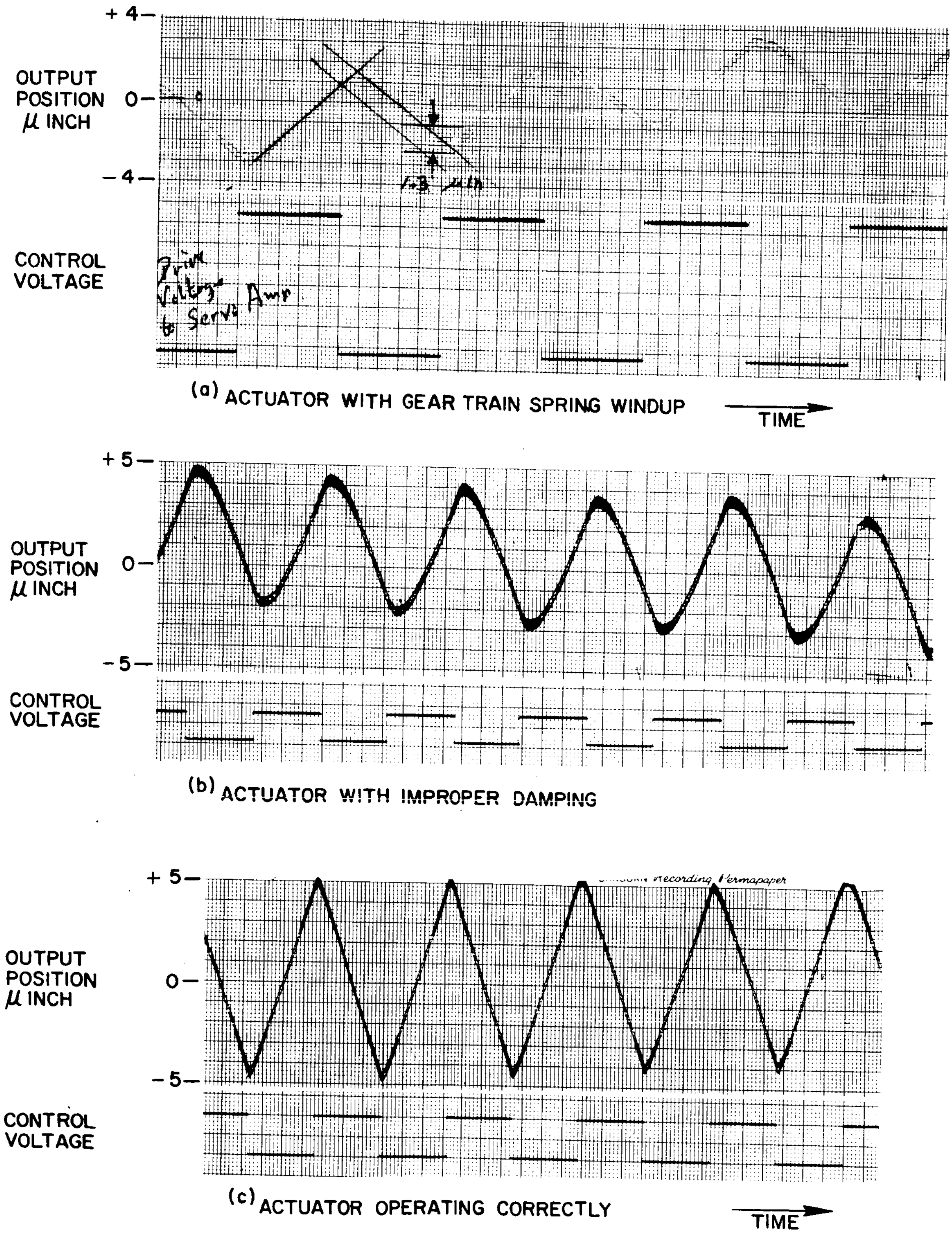

Figure 13. Actuator Response

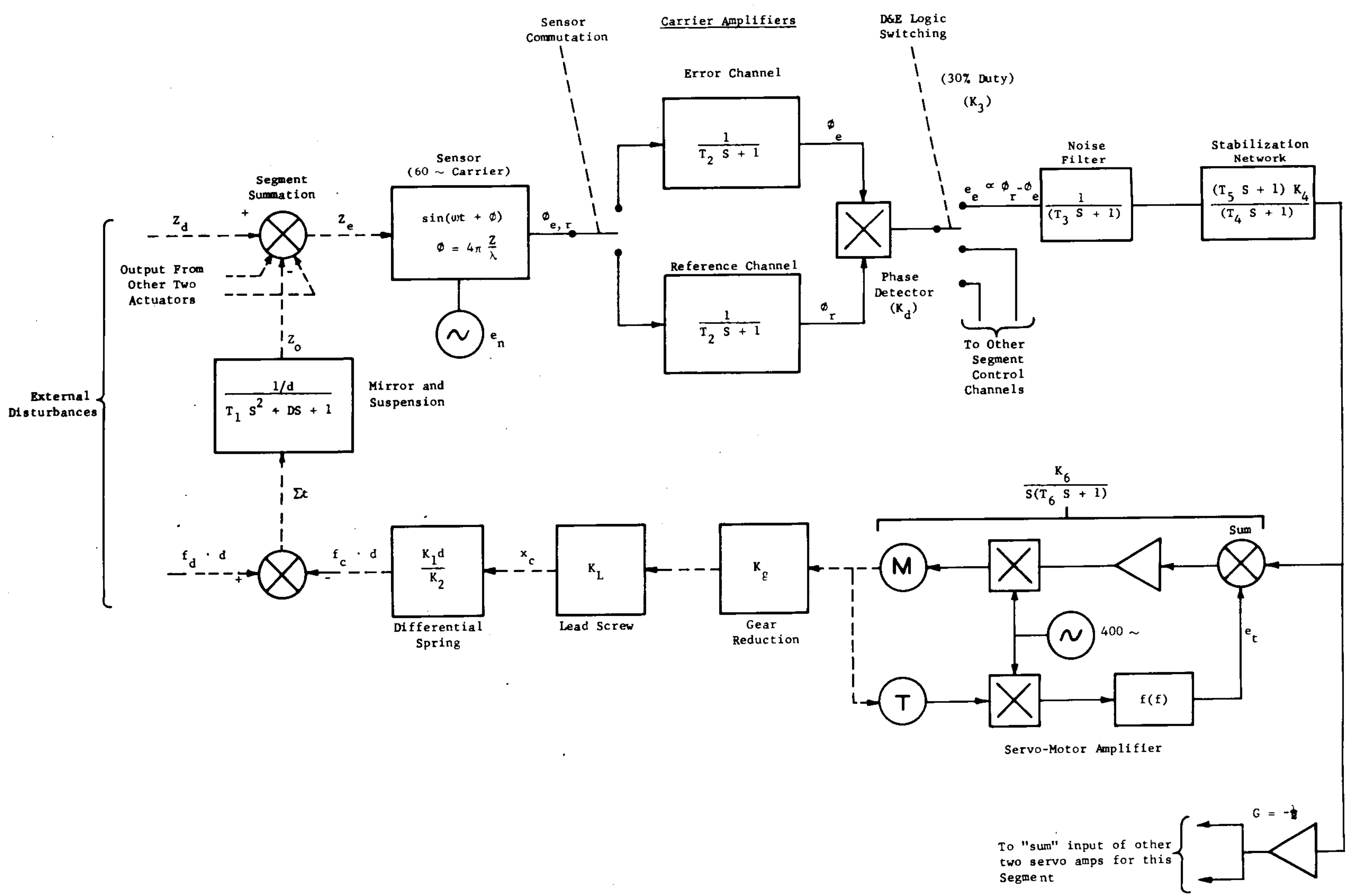

Figure 14. Servo Control Loop Diagram for One Tilt Channel

The signal is then attenuated by a factor of three because of the time sharing of the scanner between the three segments, which occurs at a 30 percent duty cycle per segment. Thus $K_3 = 1/3$. This time sharing is controlled by the D and E logic.

It was found in the earlier experiment that a noise filter is required with a break point at approximately 1 Hz to avoid photon noise for the particular laser illumination and image dissector scanner used. However, the error voltage is pulsed at this point in the system because of D and E logic switching, which made it necessary to increase the time constant of the noise filter to $T_3 = 0.5$ second.

The next element in figure 14, the stabilization network, is a lag-lead filter. The lag provides a long time constant for transient immunity and the lead is necessary as phase compensation to prevent excessive phase shift in the overall loop. The ratio of T_5/T_4 was selected to maintain the calculated open-loop phase response below 135° for frequencies below the zero gain point. A phase margin of 45° was needed because of the uncertainty in the actuator response.

The stabilization network also contains a gain factor, K_4, which is used to adjust overall control loop gain. A final selection of control loop gain is made by adjusting the value of K_4 for acceptable square wave response. The K_4 gain factor is set at unity in the tilt channels for initial alignment and is automatically reduced to 0.1 when alignment is correct. Values of K_4 for focus and axial channels are fixed at 0.1 and 0.4 respectively.

The servomotor amplifier minor loop is identical to the original design. It has a frequency response out to 22 Hz and therefore has little effect on the closed-loop operation. The gain constant for the gear train, lead screw, and differential spring are also unchanged. Therefore:

$$\frac{K_6}{S} = \frac{26}{\omega} \; \frac{\text{rev}}{\text{sec} \cdot \text{vdc}} \quad \text{(servomotor amplifier)}$$

$$K_g = \frac{1}{227} \text{ dimensionless (gear train)}$$

$$K_L = \frac{1}{40} \; \frac{\text{in.}}{\text{rev}} \quad \text{(lead screw)}$$

$$\frac{K_1}{K_2} = \frac{1}{170} \text{ to } \frac{1}{225} \text{ dimensionless (differential spring)}$$

Note that the stabilization network for a tilt loop feeds all three servomotor amplifiers for the particular segment, one servo with a ±1.0 signal and the other two with a -1/2 signal. This provides the push-pull tilt control described earlier.

The mirror suspension is such that one actuator rotates the mirror about a line intersecting the other two actuators, where the distance (d) between the axis of rotation and the actuator point of contact is 4.25 inches. The resonant frequency of the mirror suspension was calculated to be approximately 22 Hz and measured to be closer to 30 Hz, thus it also has little effect on the closed-loop servo stability. It was found that damping of the mirror suspension was not sufficient. This was corrected by the addition of silastic putty to the actuator springs.

The open loop tilt channel response can be written as:

$$Z_o(S) = 2 \times \frac{\phi_e(S) \cdot K_d \cdot K_3 \cdot K_4 \cdot \left(T_5S+1\right) \cdot K_6/S \cdot K_g \cdot K_L \cdot K_1/K_2}{\left(T_2S+1\right)\left(T_3S+1\right)\left(T_4S+1\right)\left(T_6S+1\right)\left(T_1S^2 + DS + 1\right)} \qquad (1)$$

where:

$s = j\omega$

T_n = time constant

K_n = gain factor

D = damping factor

By inserting the measured values for the constants (table II) into this expression and solving for the velocity constant, the following is found:

$$G(\omega)_{dc} = \frac{Z_o(\omega)}{Z_e(\omega)}$$

$$= \frac{2.4}{\omega}$$

From this, the frequency, f_o, for $G(\omega)_{dc} = 1$ is:

$f_o = 0.37$ Hz

f_o is located on Fig. 15 by the intersection of the zero gain line with an extrapolation of the very low frequency response curve. The calculated open-loop gain and phase characteristics of a typical tilt control channel are shown in figure 15. A Nichols chart plot of the data in figure 15 indicates that the closed-loop unit-step response should have less than 20% overshoot.

TABLE II

NUMERICAL VALUES FOR EQUATION (1)

Component	Term	Value
Figure Sensor	$\phi_e(S)$	$5 \times 10^4 \times Z_e(\omega)\ \frac{\pi\text{rad}}{\text{in.}}$
Phase Detector	K_d	5.7 Vdc/π rad
Logic Switching	K_3	1/3 (dimensionless)
Servo Amplifier	K_6/S	26/ω rev/sec · Vdc
Stabilization Network	K_4	1/10 focus channel 2/5 axial channel 1/10 tilt channel
Gear Reduction	K_g	1/227 (dimensionless)
Lead Screw	K_L	1/40 in./rev.
Differential Spring	K_1/K_2	1/170 to 1/225 (dimensionless)
Mirror Suspension	T_1	0.005 sec.
Carrier Amplifier	T_2	0.004 sec.
Noise Filter	T_3	0.5 sec.
Stabilization Network	T_4	10 sec.
Stabilization Network	T_5	3 sec.
Servo Amp/Motor	T_6	0.007 sec.

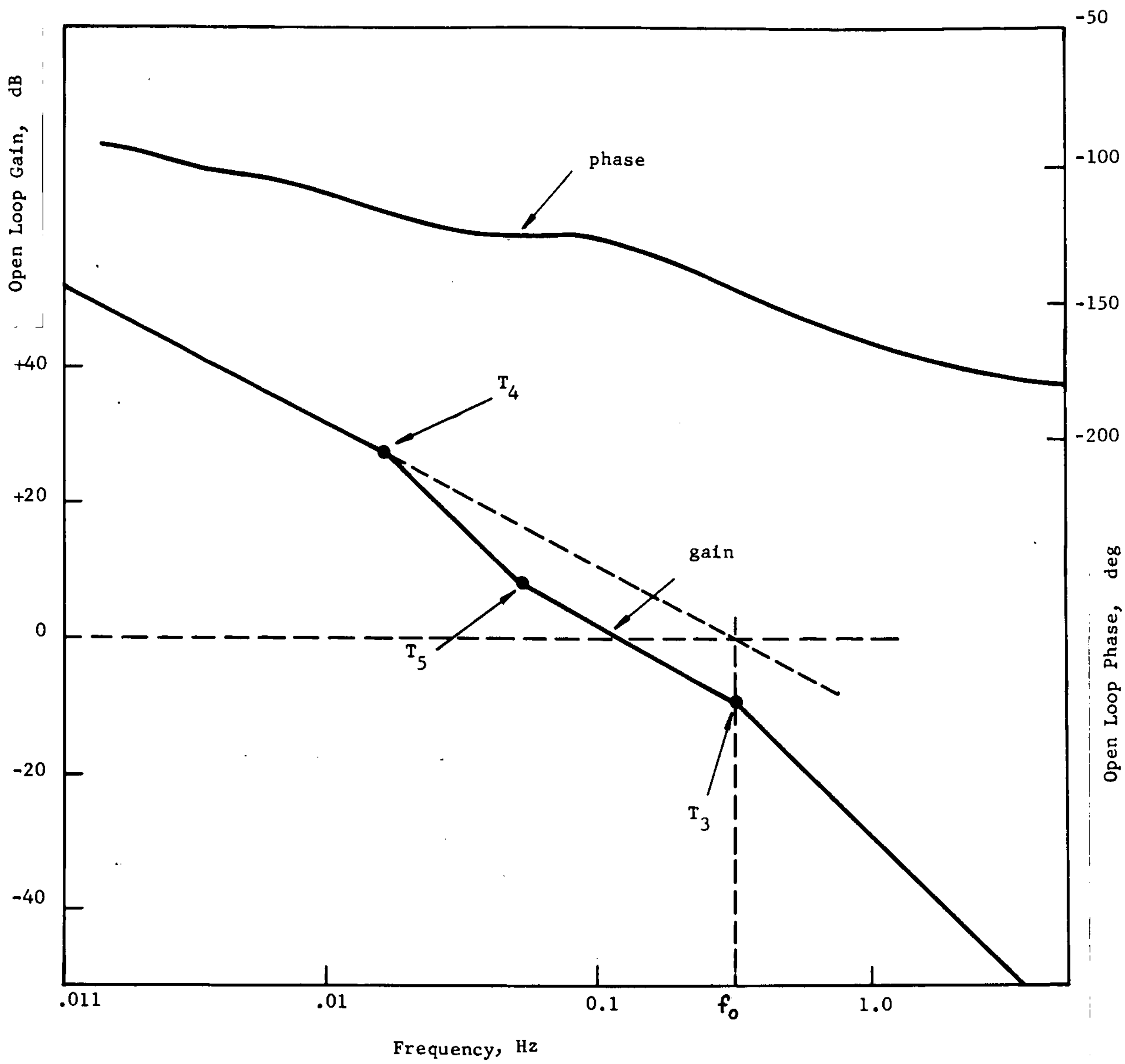

Figure 15. Control Loop Bodie Diagram

4.4 OPERATION

In principle, complete alignment could be controlled by six manual switches. These are switches MS-1 through 4, 7, and 8, whose functions are listed in the lower left corner of figure 4 (sheet 1 of 2). The actual breadboard contains several more switches which were incorporated as a convenience during "debugging" and performance measurements.

The sequence of alignment is started by closing switches MS-1 and MS-2. A small alignment-error sensing scan begins for each segment. Tilt alignment occurs at a rapid rate at the beginning. As tilt is corrected for all three segments, the scan size increases, tilt control rate slows down, and axial alignment errors are generated. MS-4 is then closed and focus alignment begins for segment I. This is done by switching MS-3 on and MS-7 to position No. 2, which initiates a fixed slew. To save time and prior to this step, a manual scan is made of both segments II and III to find the sense of the axial alignment error and the axial slew direction is selected with switch MS-8. Axial slew continues until the white light interferometer indicates confocal coincidence between segments I and II by closing relay RS-1. Activation of RS-1 removes the axial slew, closes the axial control loop for segment II, and reduces the tilt loop gain in channels 5 and 6 by a factor of ten. This relay is also self-locking. The same procedure is initiated for segment III by turning MS-7 to position No. 3.

5. SYSTEM PERFORMANCE

5.1 CONTROL SYSTEM TEST DATA

Signal and noise levels were measured in the electronics with results as shown in table III. Figure 16 contains recordings of the d-c error signal versus mirror position for a tilt control channel and for the raster channel. Figure 17 contains recordings, at an increased gain setting, of the d-c noise level for the same channels. Figure 18 shows the square wave response of a tilt control loop at high and low gain settings corresponding to $K_4=1.0$ and 0.1. Data for the focus channel is not presented because the noise levels are very much smaller and the response time is on the order of many minutes.

Figure 19 shows the response of the system to external transients. These transients were introduced by a 160 lb person leaning heavily on the vacuum tank and then releasing his weight suddenly. It can be seen that the control system is not disturbed significantly and recovers rapidly.

Figures 20 and 21 show a series of fringe patterns produced by the interferometer after automatic alignment.

5.2 OVERALL PERFORMANCE

Three methods of evaluation were utilized to determine the optical performance of the complete system. The first two methods provide qualitative data and the third method provides quantitative data.

5.2.1 Pinhole Photographic Recording

The first method utilized was the photographic recording of the optical image, formed by the segmented mirror, of a small light source located near the center of curvature. The nominal diameter of this source was 0.0001 inch. The image formed was magnified by a microscope of approximately 375 magnification which also re-imaged the pinhole upon the photographic film suitably mounted above the microscope. A sample of the photographs thus obtained is shown in figure 22. Figure 22a is the appearance of the separate images of the three segments when they are misaligned. Figure 22b, which is to the same scale as Figure 22a, is the single image formed by the fully aligned segments. In this figure the overall performance of the system can be observed. The relative size of the aligned image compared to the individual segments, indicates the achievement of higher resolution in a diffraction-limited image by using additional reflecting surfaces properly aligned with the first surface. The diffraction ring formed about the central maximum in Figure 22b, indicates that the mirror exhibits minimal large-scale figure errors. This indicates that not only are the individual segments of good figure, but also the control system is maintaining very good alignment.

TABLE III

SIGNAL AND NOISE LEVELS

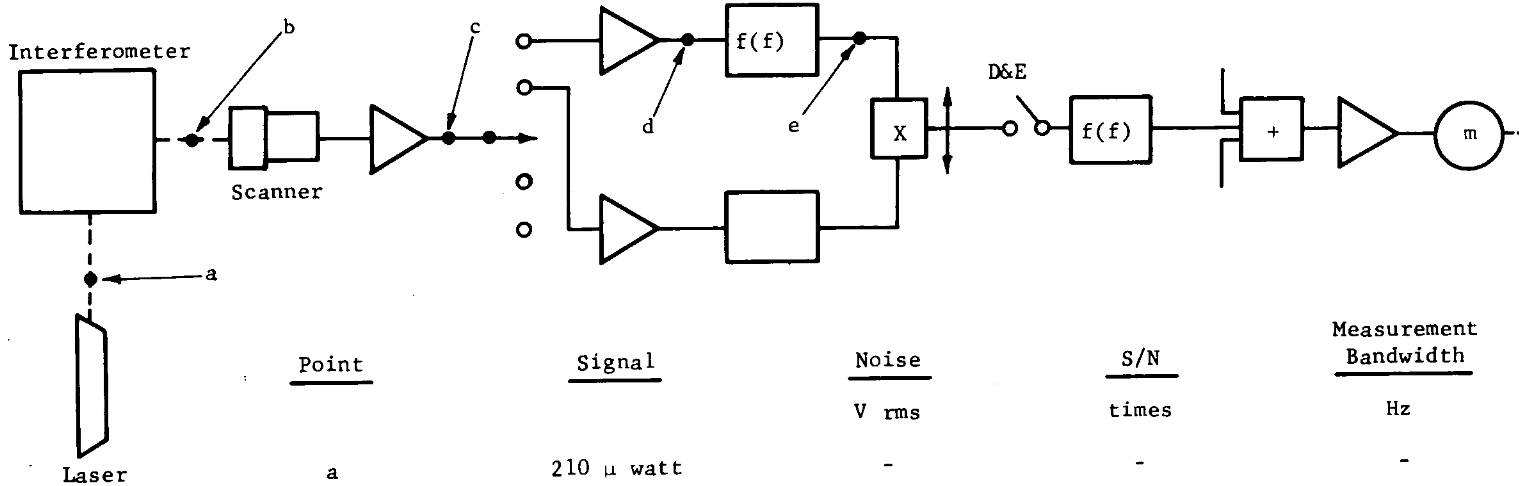

Point	Signal	Noise	S/N	Measurement Bandwidth
		V rms	times	Hz
a	210 μ watt	-	-	-
b	60 μ watt	-	-	-
c	1.0 V rms	0.033	31	200
d	1.0 V rms	0.075	13.5	200
e	0.48 V rms	0.025	19	100

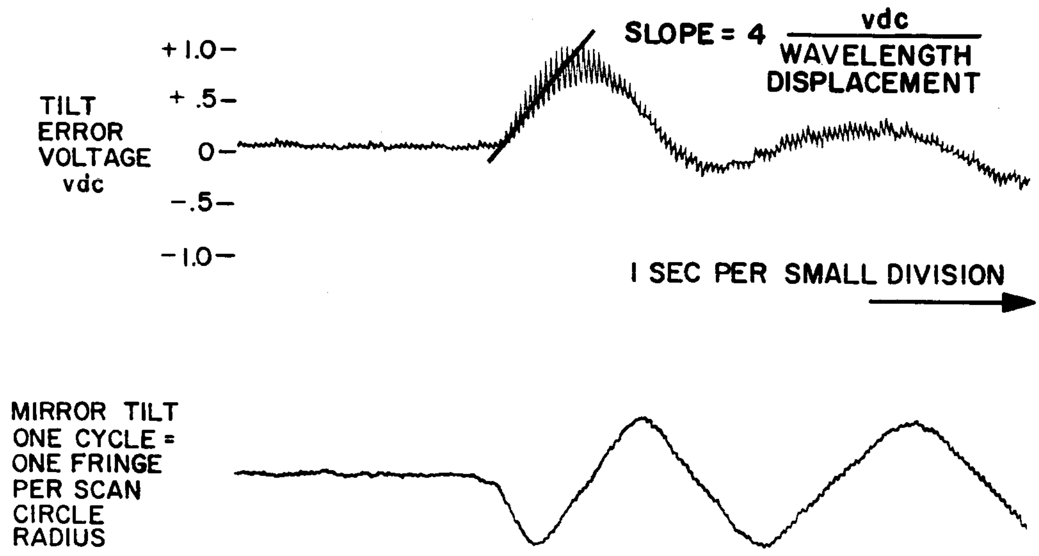

(a) ERROR VOLTAGE vs TILT FOR A FIXED SIZE CIRCULAR SCAN.

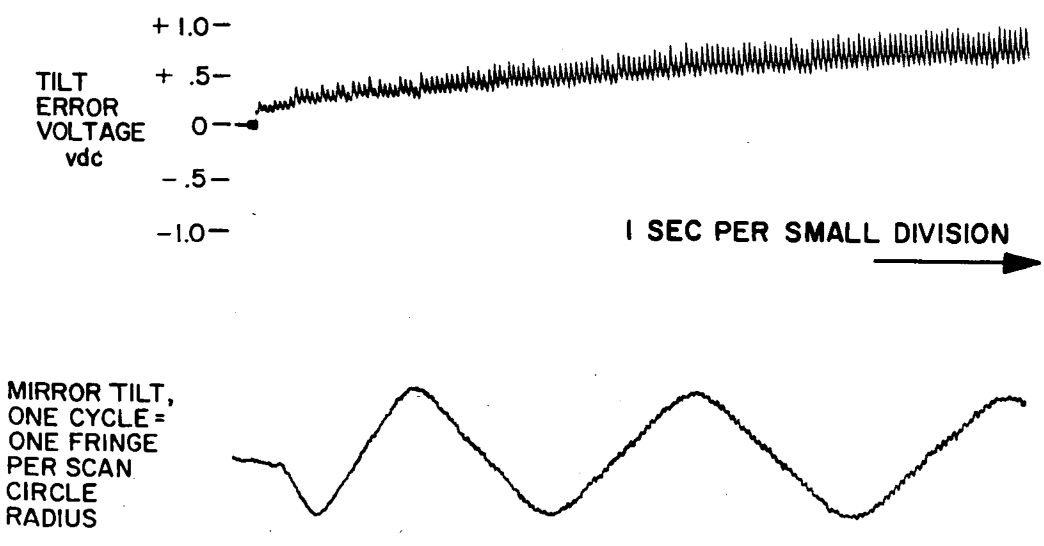

(b) ERROR VOLTAGE vs TILT FOR CIRCULAR SCAN DIAMETER CONTROLLED BY AN AGC

Figure 16. DC Error Signals, Tilt, Axial, and Raster Channels

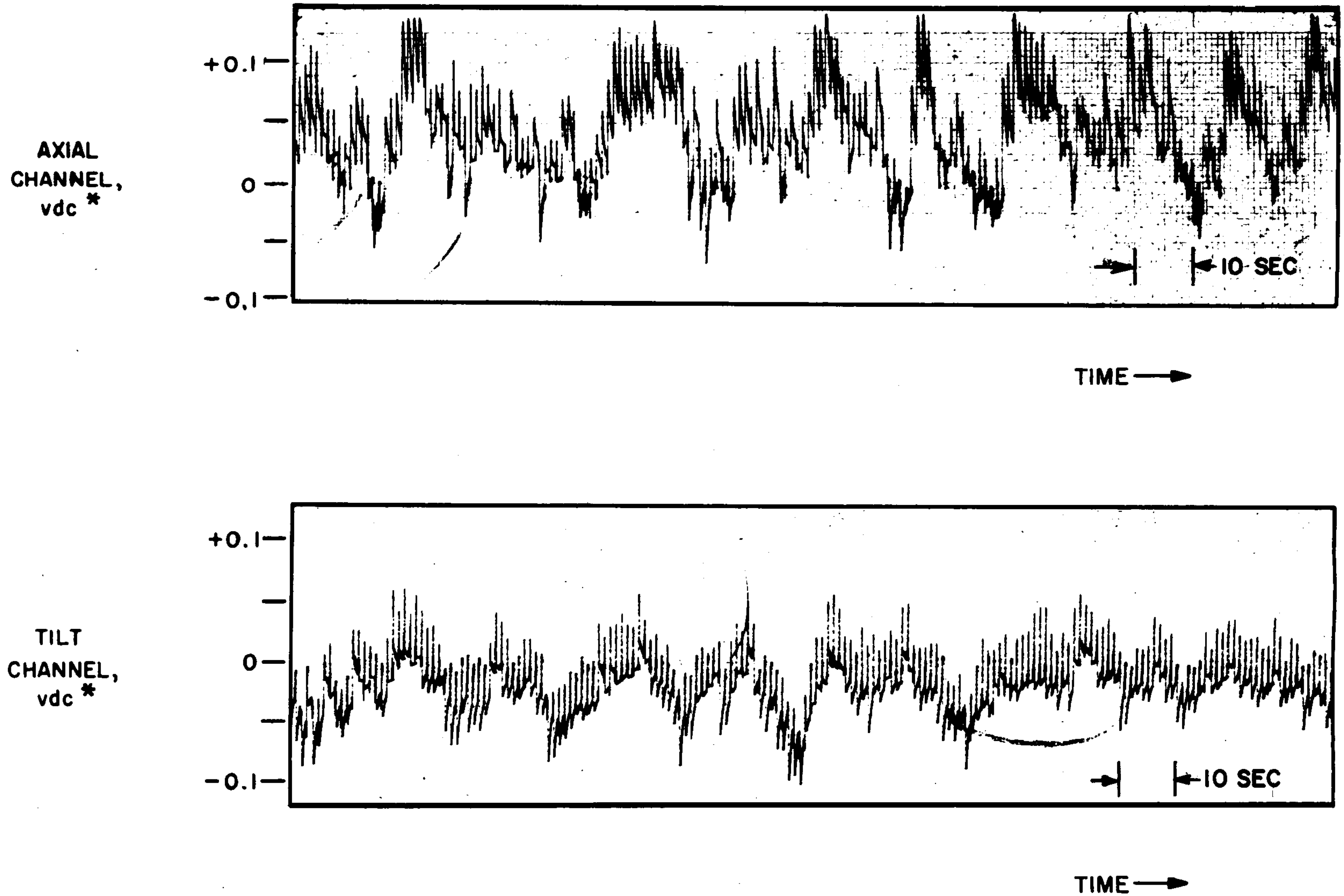

* 1 VOLT ERROR SIGNAL EQUIVALENT TO 0.25 WAVELENGTH MIRROR DISPLACEMENT

Figure 17. DC Noise Levels, Tilt, Axial, and Raster Channels

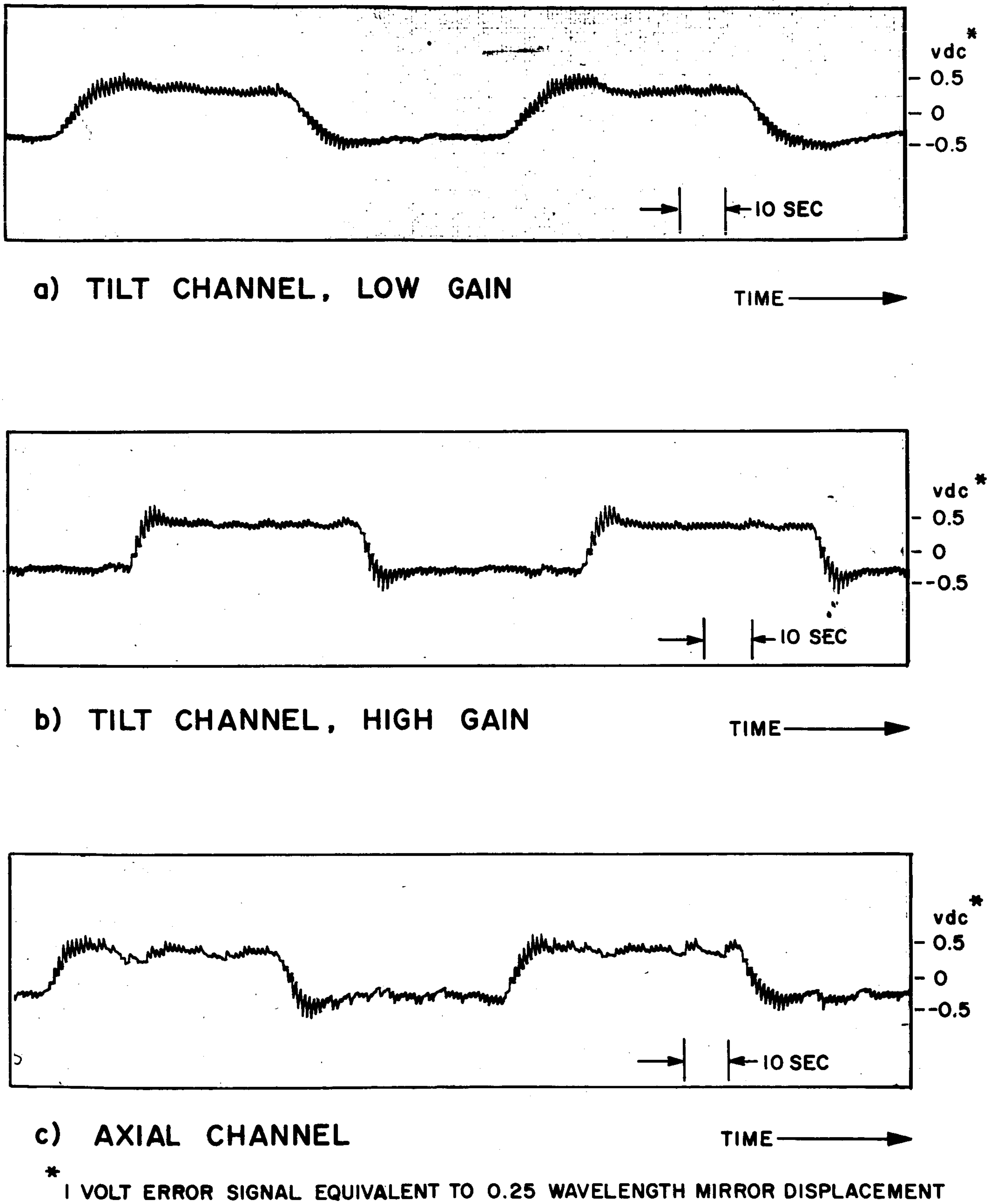

Figure 18. Square Wave Response, Tilt and Axial Channels

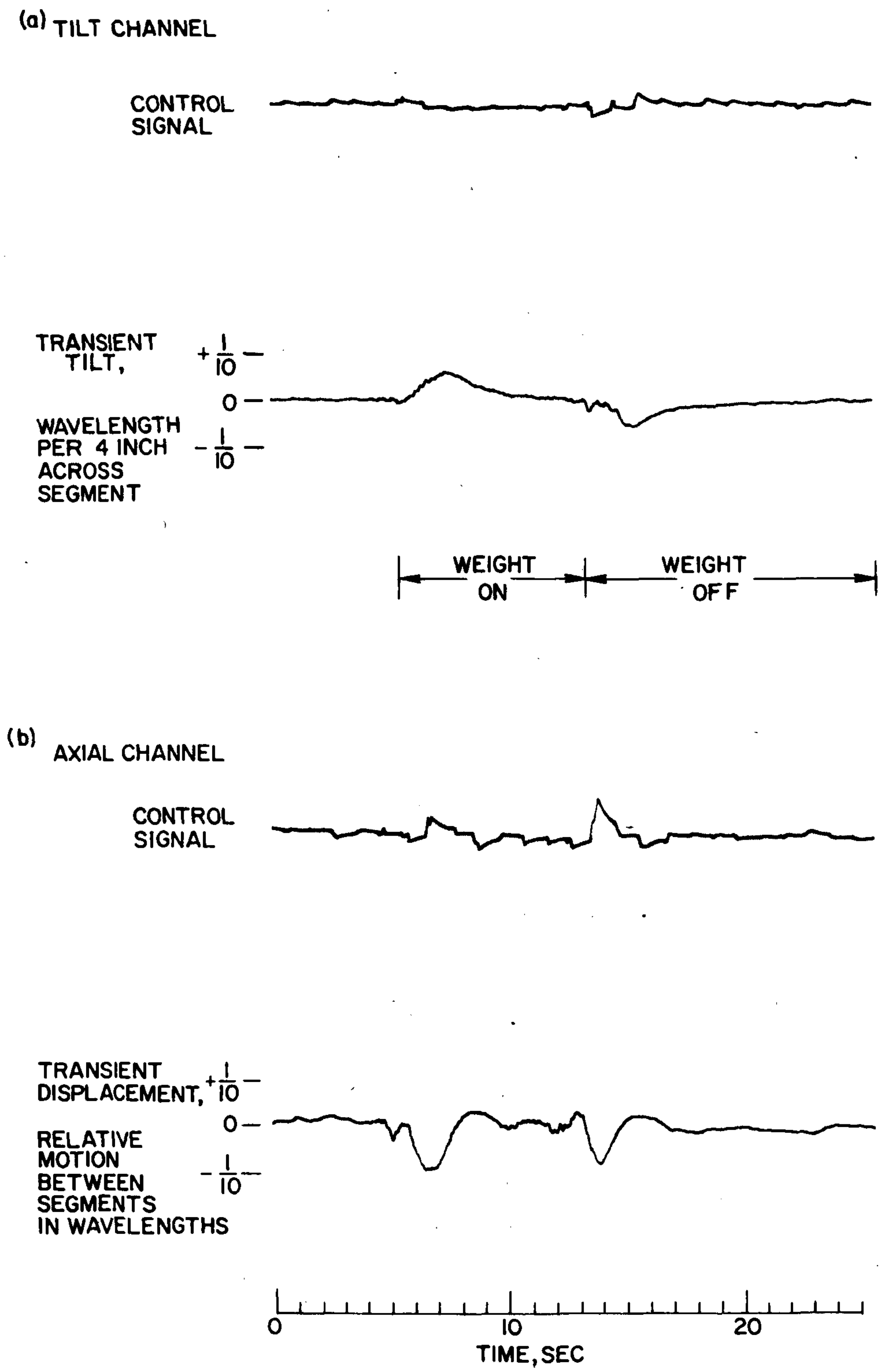

INPUT TRANSIENT WAS WEIGHT OF A 160 lb MAN APPLIED TO ONE CORNER OF VACUUM TANK ASSEMBLY

Figure 19. External Transient Response

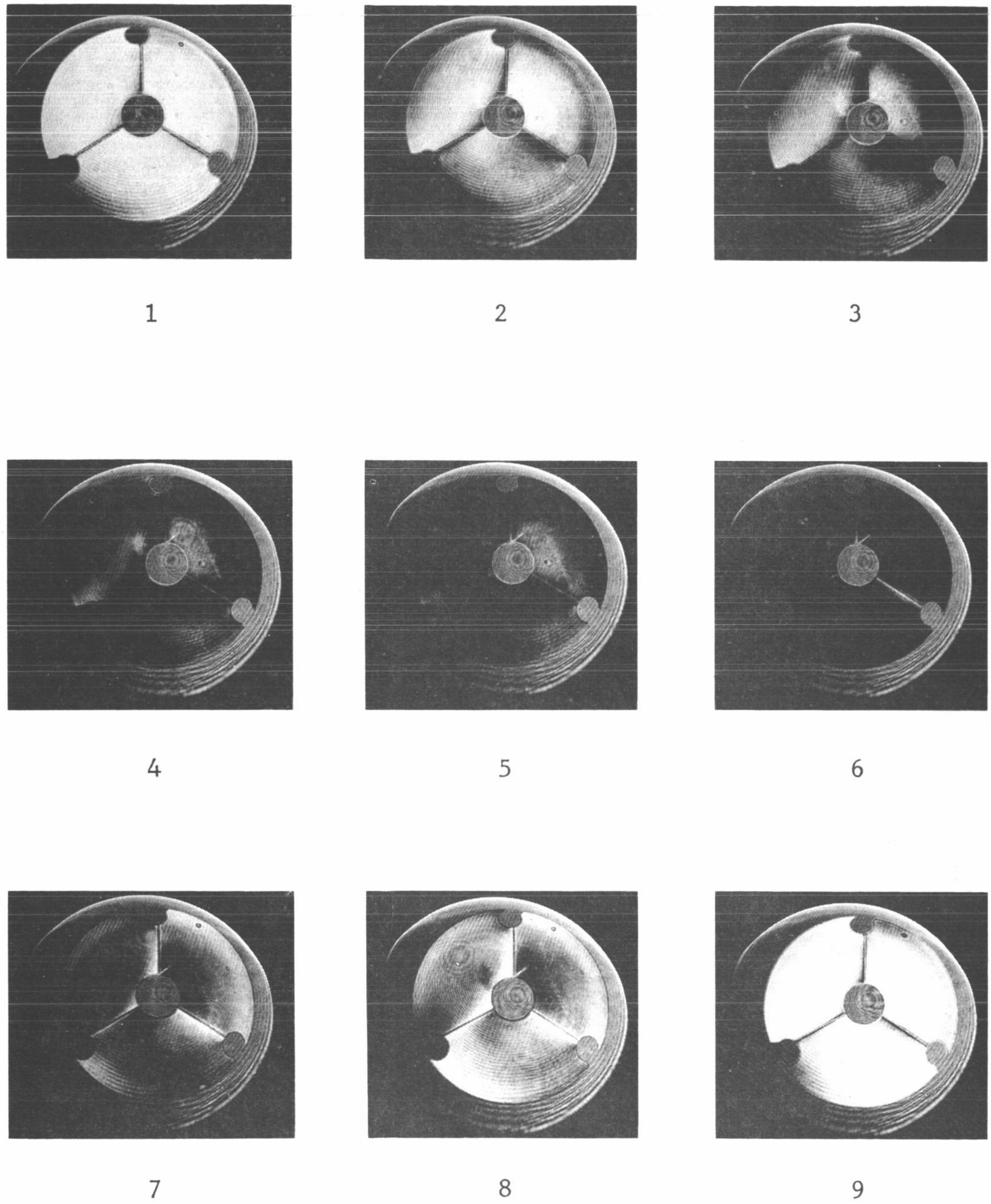

Figure 20. Fringe Patterns After Automatic Alignment (Numbers refer to sequential angular positions of the phase shifter 1/4 wave plate.)

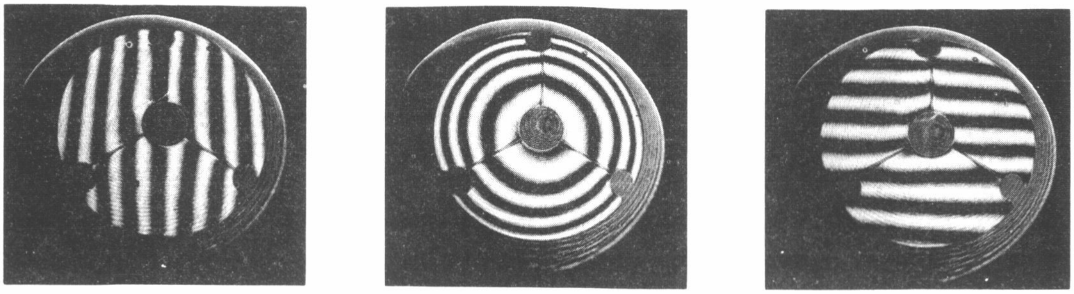

Lateral Off-set | Axial Off-set | Lateral Off-set

Figure 21. Fringe Patterns After Automatic Alignment (Pictures taken with phase shifter motor off and manual off-set of de-collimating lens in the interferometer.)

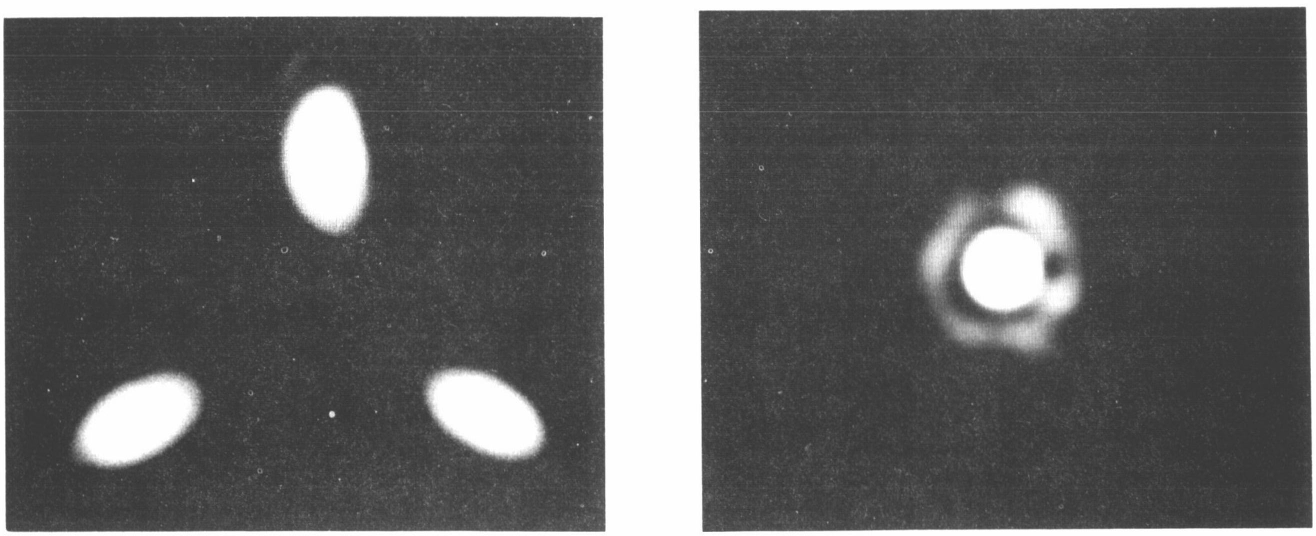

(a) Segments Misaligned | (b) Segments Aligned

Figure 22. Pinhole Photographic Recordings

5.2.2 Foucault Test

The second method used to make qualitative measurement of the system performance was the Foucault test. In the performance of this measurement, the data was recorded photographically. Figure 23 is one of the photographs so taken. The evaluation of this data gives indication of the correct tilt alignment of the three segments. Any apparent tilt error of a given segment is indicated by a difference in the brightness of the image of that segment as compared to the segment to whose tilt it is being compared. The equal intensity of the three segments in the photograph indicates very good tilt alignment about the axis for which this measurement was sensitive.

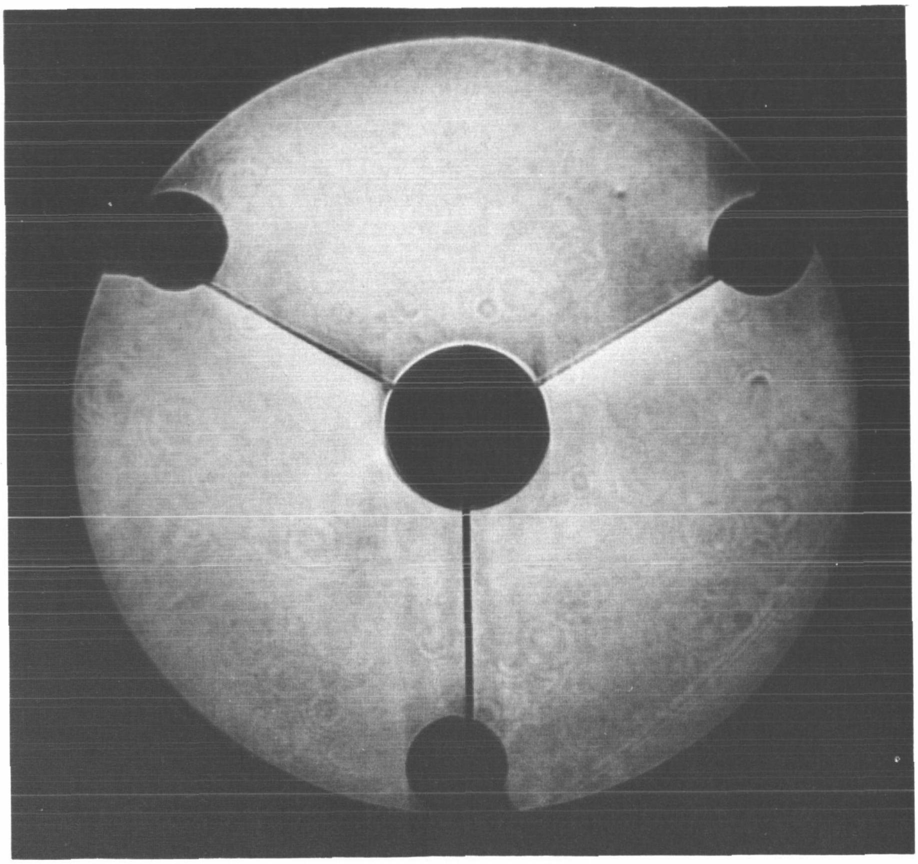

Figure 23. Foucault Test Photograph

5.2.3 Raster Scan

The profile of the mirror figure errors, as indicated by phase shift in the interference pattern at the output of the phase measurement interferometer, was plotted on an X-Y recorder. Two sets of profile scans recorded in superposition are shown in figure 24. Figure 25 shows the result of the average of four sets of profile scans. The profiles were obtained by measuring and plotting the difference in phase between a scanning spot and a reference spot using the same type of phase detector used in the control system and feeding the result to the X-Y recorder with a filter time constant of 1/3 second. Each line scan took approximately one minute and each raster was completed in approximately one half hour. The superposition of two scans (figure 24) shows the stability of the control system. Segment I appears more stable than segments II and III because the reference point is on segment I and the only variations are caused by motions in tilt. The variations seen in segments II and III include errors of tilt and of axial position relative to segment I. The variation appears to be random with no cyclic component detectable. The largest peak-to-peak variation is 1/30 wavelength, which would indicate an rms positioning stability of approximately 1/150 wavelength. The area under the curves in segments I, II and III were calculated and averaged, furnishing the following results:

	Average Deviations
Segment I	$\lambda/60$
Segment II	$\lambda/55$
Segment III	$\lambda/90$
Total composite mirror	$\lambda/64$

Some slight improvement might be made in these averages by a slight shift in reference obtained by a control scan which covers the triangular segment more completely than the present circular scan or by biases applied to the segments. The circular scan, however, would be an effective one for more symmetrical segments as might be used in a seven or more segment mirror. The raster scans shown in this report do not include any portion of the rolled down edge which is outside the 20-inch diameter for which the mirror was figured, as this area was masked out. Some of this rolled down edge was included in the profile scan shown in figure 42 of the Final Report (Perkin-Elmer Report No. 8525) and this partly accounts for the improvement in the average figure error calculated for figure 25.

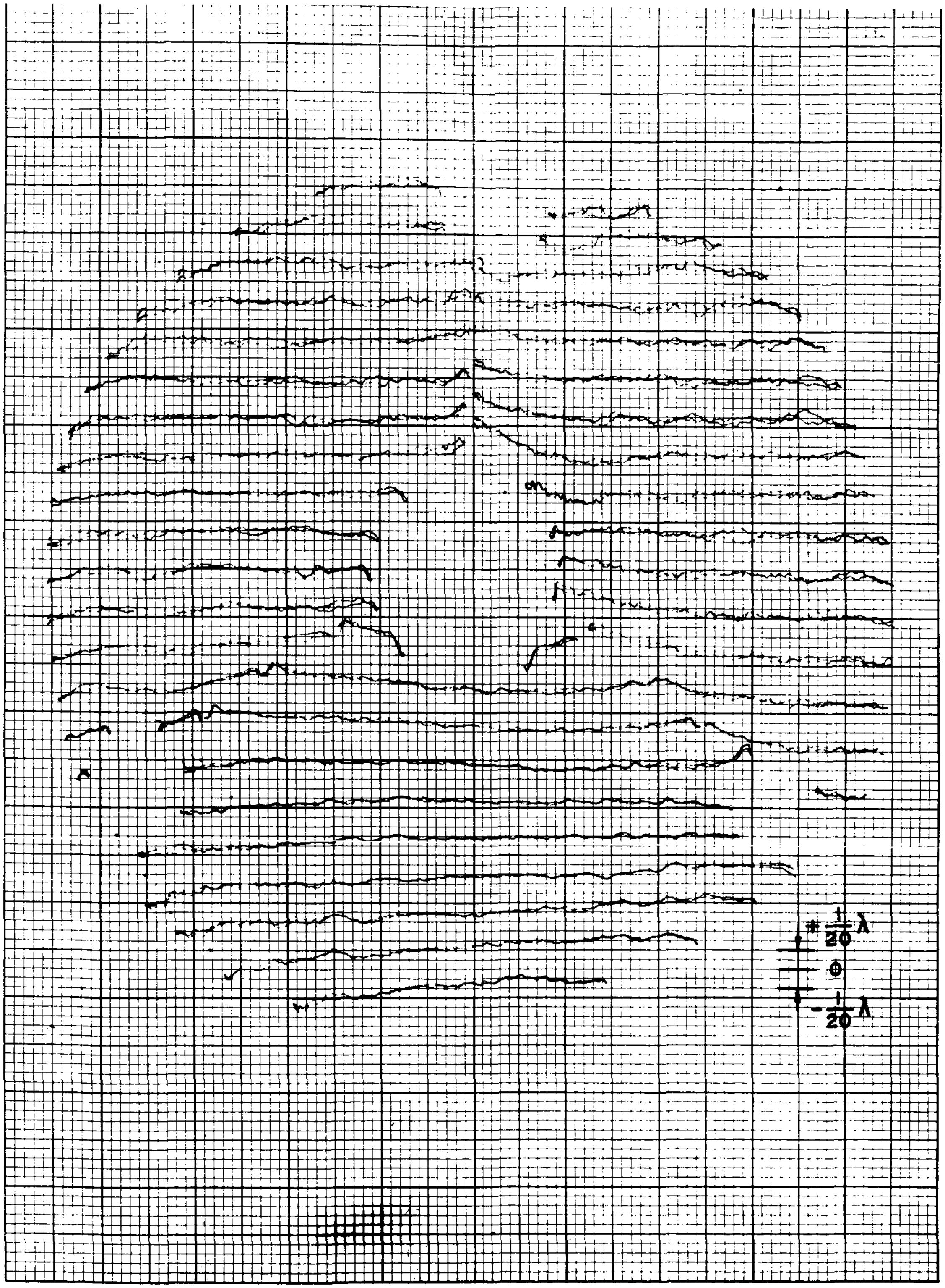

Figure 24. Raster Scans

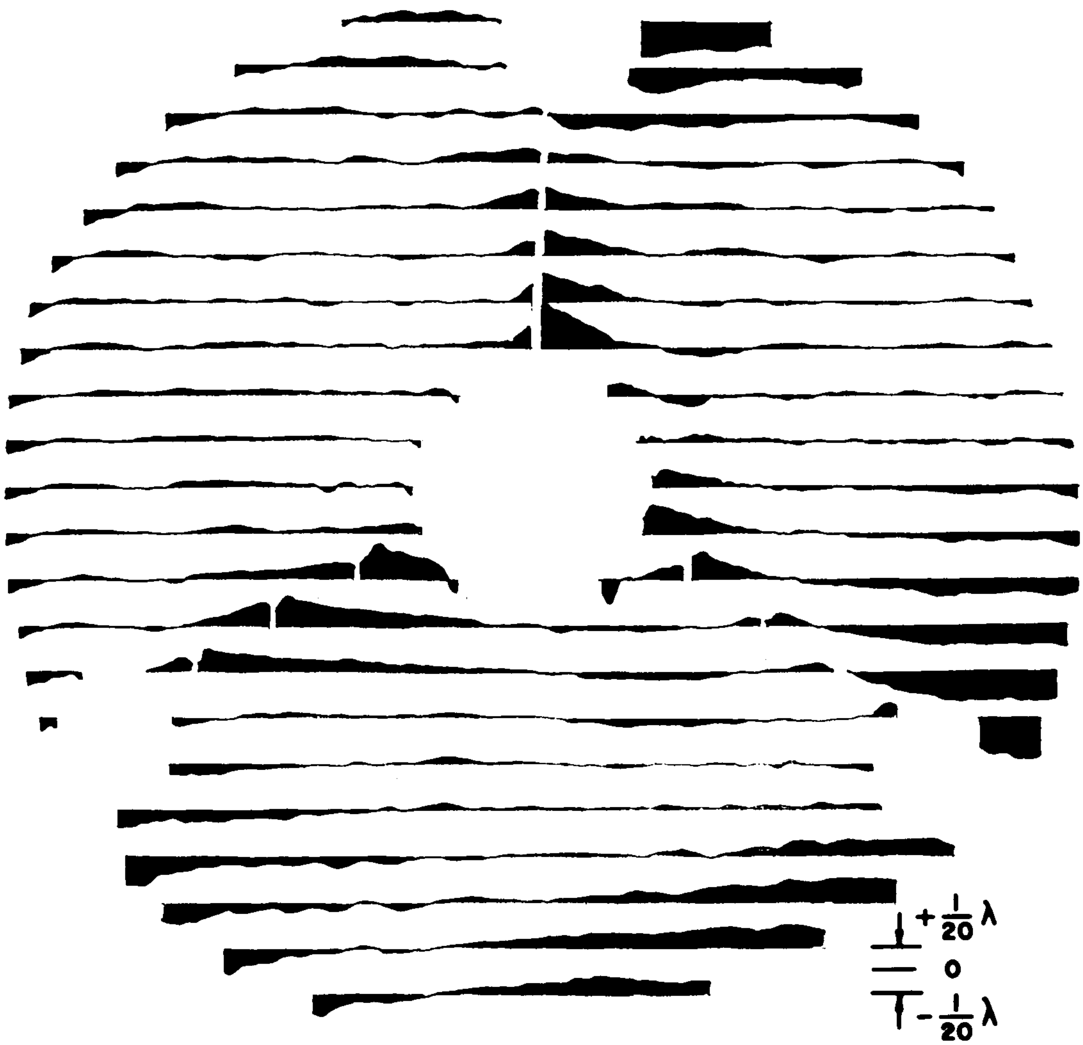

Figure 25. Raster Scan Average

5.3 FUNDAMENTAL LIMITS

The fundamental limits of performance in an electro-optical control system may be related to the error sensor characteristics and the system response time. If very high gain is used in the feedback loop these are the only limits of performance. Where loop gain must be reduced for stability reasons, other sources of error may become significant.

The limits of performance may be categorized as:

1) Accuracy.
2) Stability.
3) Dynamic Range.
4) Response Time.

Table IV lists those limits of performance encountered in the experiments and those anticipated as fundamental to this type of control system.

Accuracy was limited by the individual segment figure errors, as can be seen be reference to figure 25. The use of a circular scan in the figure sensor minimized the response to local high or low spots; however, the system could be further optimized by averaging over the entire segment.

Figure sensor components were discussed in section 3. The data indicates that the figure sensor errors, as averaged by the circular scan, are less than 1/50 wavelength. Some spurious fringe patterns remain (see figure 20); however, these are either averaged out by the circular scan or originate outside the two interference beams and hence produce intensity effects only and not phase errors.

An objective of this phase of the work was to incorporate space and time averaging of all alignment errors to minimize spurious effects such as figure sensor errors and transient vibrations. The insertion of a long time constant filter in the control loop made it necessary to reduce overall gain to insure stable operation. The only convenient place for gain reduction was in the stabilization networks. The result was that d-c drift in the servo amplifiers following the filter would, at times, affect overall accuracy.

The fundamental limits of accuracy are the segment figure errors and the phase detector measurement capability. An electronic phase detector is capable of resolving relative phase to better than two degrees, which corresponds to better than 1/100 wavelength. Thus the segment perfection is the actual fundamental limit of performance in a segmented Active Optics system.

In principle, photon noise in the laser beam of the figure sensor should determine the short term stability. Table III shows that the magnitude of photon noise, as limited by the filters used, is less than 10° peak-to-peak, or 2° rms. This corresponds to less than 1/400 wavelength rms.

TABLE IV. PERFORMANCE LIMITS

	Accuracy	Stability	Dynamic Range	Response Time
Present Experiment	Segment Figure Figure Sensor Components ($\lambda/50$) Servo Amplifier Drift	Vibration Air Turbulence ($\lambda/150$ rms) Photon Noise ($\lambda/400$ rms)	Circular Scan Diameter (5 fringes per segment) Actuator Range	Control Loop Stability
Fundamental Limits	Segment Figure Phase Detector Accuracy ($\lambda/200$)	Photon Noise Thermal Drift in Figure Sensor ($\lambda/40$ per hour)	Scanner Aperture (50 fringes per segment)	Anticipated Thermal Perturbations

During Phase I of the project, it was found that overall stability could be affected considerably by vibration and air turbulance in the figure sensor. Precautions were taken to minimize both in the final experiment. These effects were proportional to the distance between the point of interest and the reference spot. For alignment of segments II and III, turbulance and vibration predominate over photon noise by a factor of two to three times. For segment I alignment, photon noise predominated.

Long term stability is related to the thermal stability of the figure sensor. The long term drift of the figure sensor mounted on a cast iron optical test bench has been measured as low as 5 deg/hr, corresponding to 1/40 wavelength at the mirror. Using the aluminum base plate phase measurement interferometer, which is physically mounted on the vacuum tank, the thermal drift rate increased to a value of 1/10 wavelength per hour.

Dynamic range of automatic alignment control is limited by the number of fringes that can be detected. This is determined by the minimum scan diameter and scanner aperture diameter. Measurements on the experimental breadboard indicate that up to five fringes per segment could be accommodated automatically. In principle, the system could be designed to accommodate up to 50 fringes per segment.

The response time, which can be designed to any value greater than approximately one second, is approximately five seconds (see figure 18). Practical considerations in the experimental breadboard precluded use of a longer time constant. However, this was adequate for the system to accommodate fairly severe transients as shown by reference to figure 19.